LAWRENCE
LIVERMORE
NATIONAL
LABORATORY

LLNL-TR-664386

Design of a Large Diffraction Grating Optical Assembly

J. Galbraith

November 18, 2014

Disclaimer

This work performed under the auspices of the U.S. Department of Energy by Lawrence Livermore National Laboratory under Contract DE-AC52-07NA27344.

Design of a Large Diffraction Grating Optical Assembly

Justin Galbraith

MS Plan II Technical Report

University of California, Davis

November 18, 2014

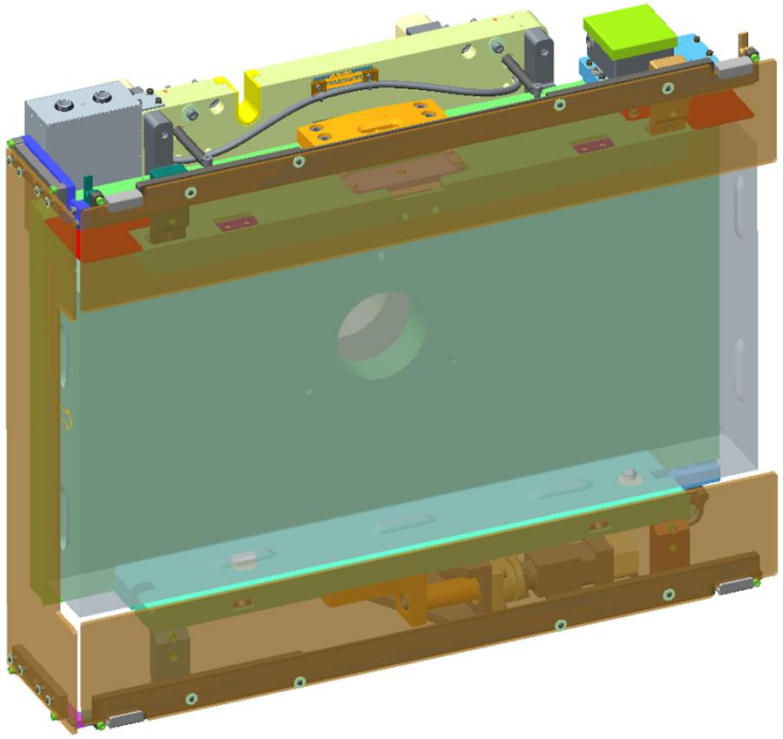

LLNL-TR-664386

Table of Contents

Acknowledgements

The success of the Grating LRU project was possible only through the combined effort of a large engineering team. In particular, Matt Fischer, JB McLeod, Arlen Rowe, Travis Lange, Dain Holdener, and Mike Dailey must be commended for their outstanding contributions and critical insights.

Introduction / Scope

The Advanced Radiographic Capability (ARC) is a diagnostic system in the National Ignition Facility (NIF) that will enable high-speed imaging of imploding targets in the NIF Target Chamber. NIF is a multi-billion dollar project to focus 192 laser beams onto a small target (approximately the size of a pencil eraser) to generate nuclear fusion. The complete ARC system is composed of approximately 80 modular large optical assemblies known as Line Replaceable Units (LRUs). The total estimated weight of the ARC optics alone is 16,000 lbs, with an average optic weight of 200 lbs.

Key to the function and performance of ARC is an optical compressor, which uses diffraction gratings known as Grating LRUs to temporally compress a total of 8 laser beams. The resulting high-power beams are focused onto a back-lighter target to create high-energy x-rays for imaging. These Grating LRUs are housed inside vacuum vessels called Compressor Vessels (Figures 1-5). There are a total of 32 Grating LRUs, 16 in each Compressor Vessel.

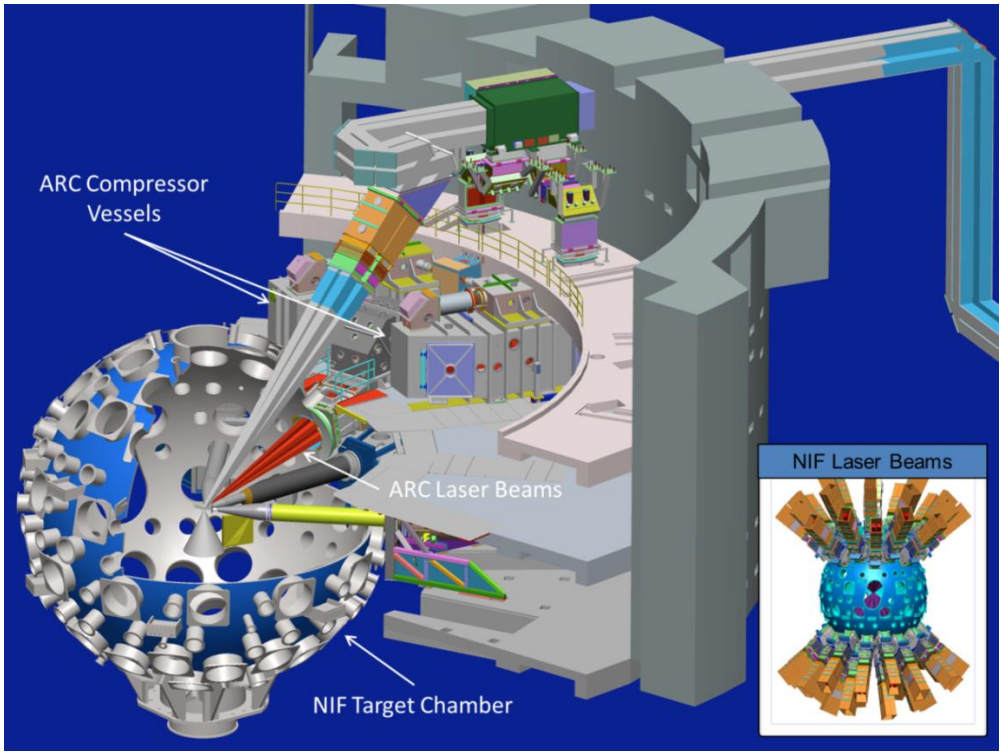

Figure 1 – ARC Laser Beams Fired into the NIF Target Chamber

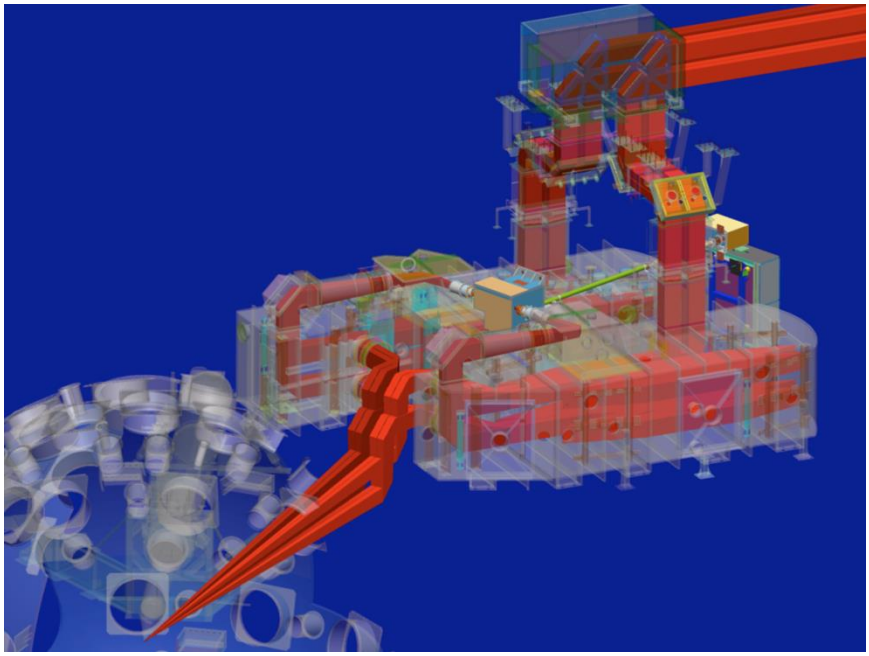

Figure 2 – ARC Laser Beampath with Translucent Vessels

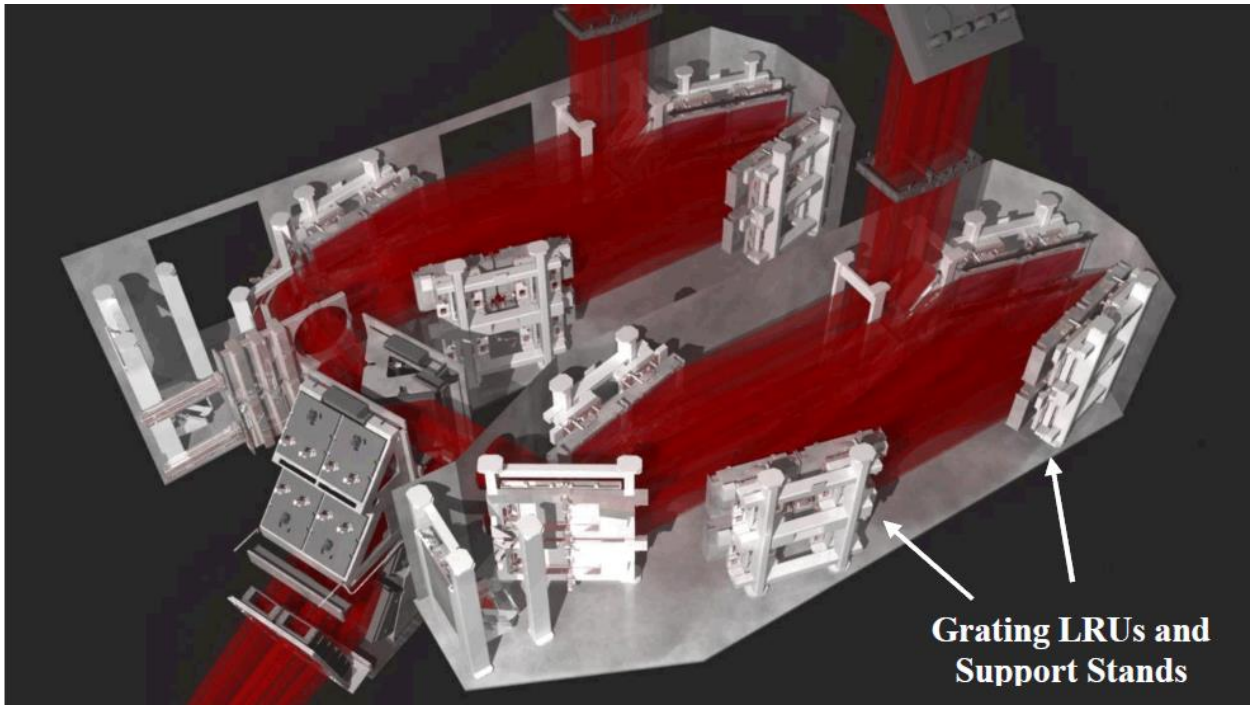

Figure 3 – Grating LRUs and Supports Stands Inside Compressor Vessels – Note Qty. 4 Grating LRUs Per Support Stand

Since accepting employment at Lawrence Livermore National Laboratory (LLNL) in 2010, I have been a primary member of the engineering team responsible for the design, assembly, testing, and commissioning of these Grating LRUs. Over the last 4 years, I have assumed additional responsibility and currently serve as the Lead Engineer for ARC LRU Systems, which includes all 80 ARC LRUs, as well as associated vessels and infrastructure. This paper will focus on the mechanical design of these Grating LRUs and will highlight a number of key feature that make the Grating LRU a unique and successful design.

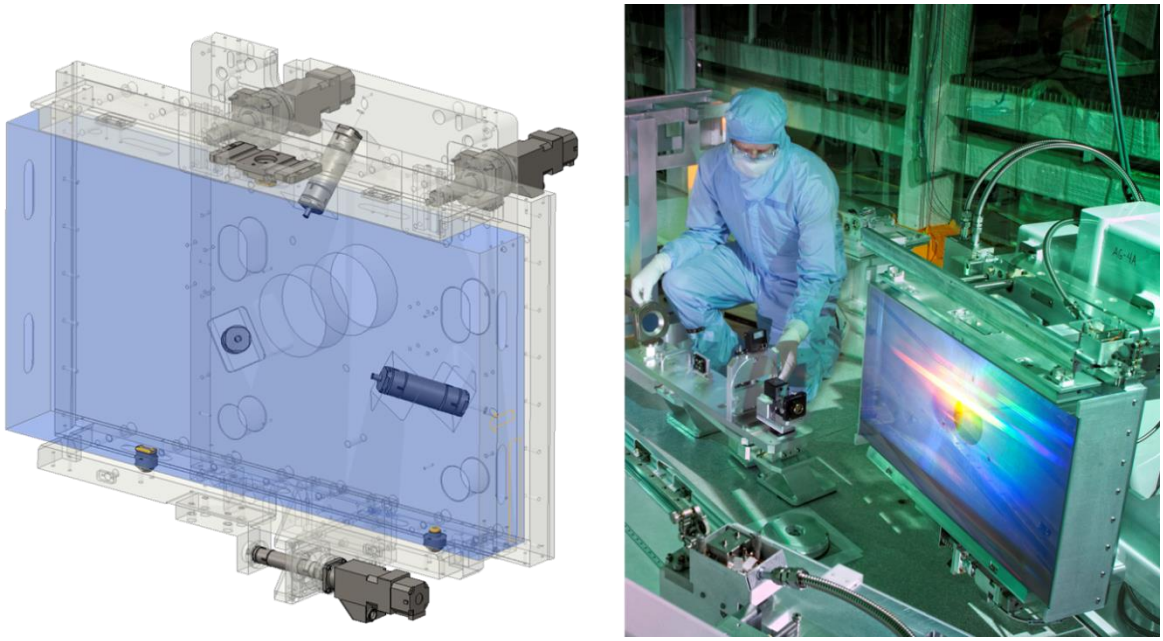

Figure 4 – Grating LRU Model (Left); Prototype Grating LRU in ARC Testbed (Right)

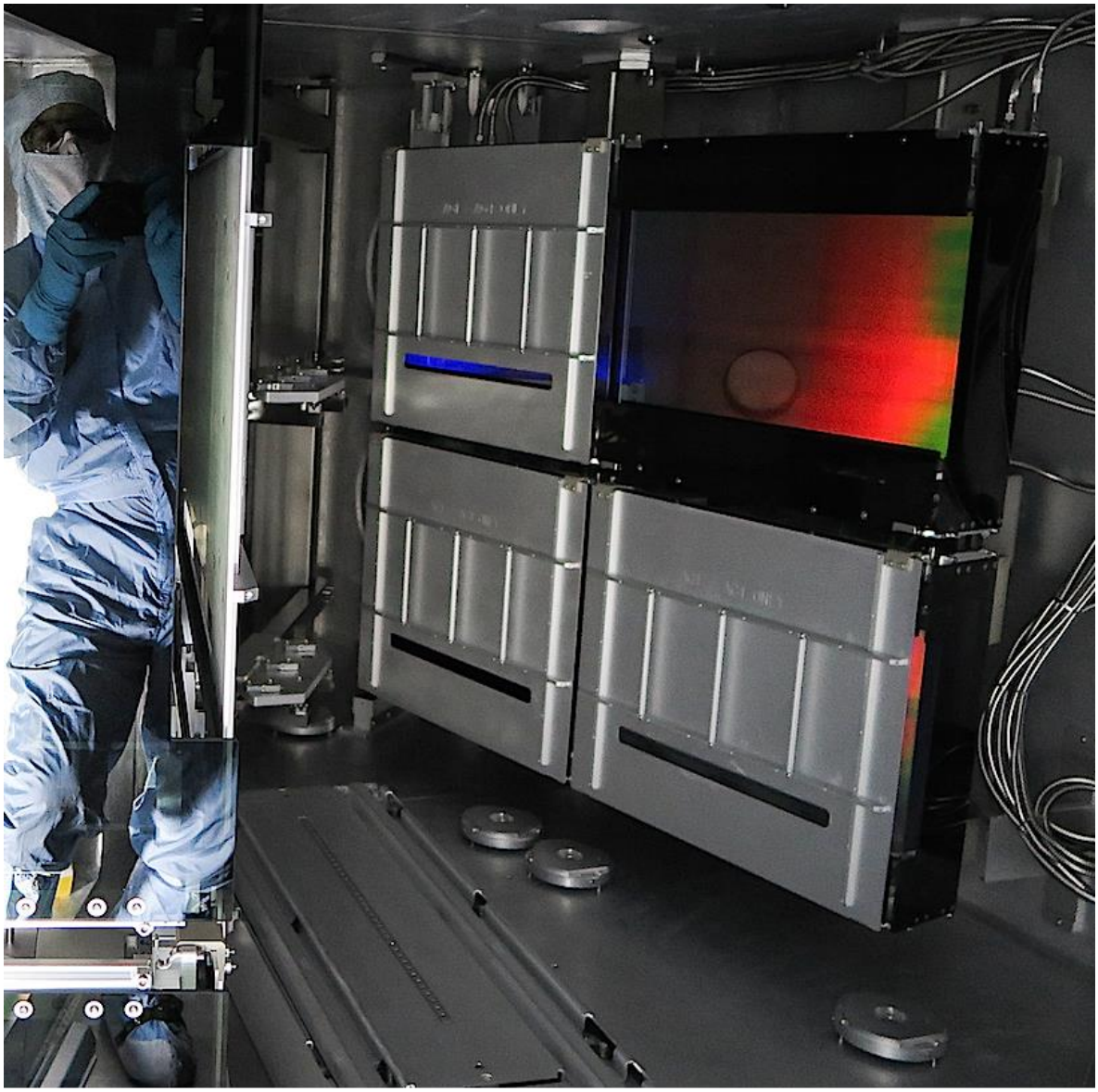

Figure 5 – A Quad of Grating LRUs Installed in a Compressor Vessel – the Operations Cover is Removed from the Upper Right LRU

Grating LRU Design

Certain elements featured in the Grating LRU design are critical to the proper function of the LRU and will be discussed subsequently. These include: optic-edge dowel support, actuated flexure system, piston adjustment mount, secondary restraint system, and ghost-mitigation armor glass.

Optic-Edge Dowel Support System

Each Grating LRU optic is supported on its edge by three dowel supports. The bottom surface has two groove features which engage one spherical and one pin dowel. The upper surface has one groove feature engaging another pin dowel (Figure 6). These three dowels constrain the optic in a deterministic, repeatable manner and function as a quasi-kinematic mount.

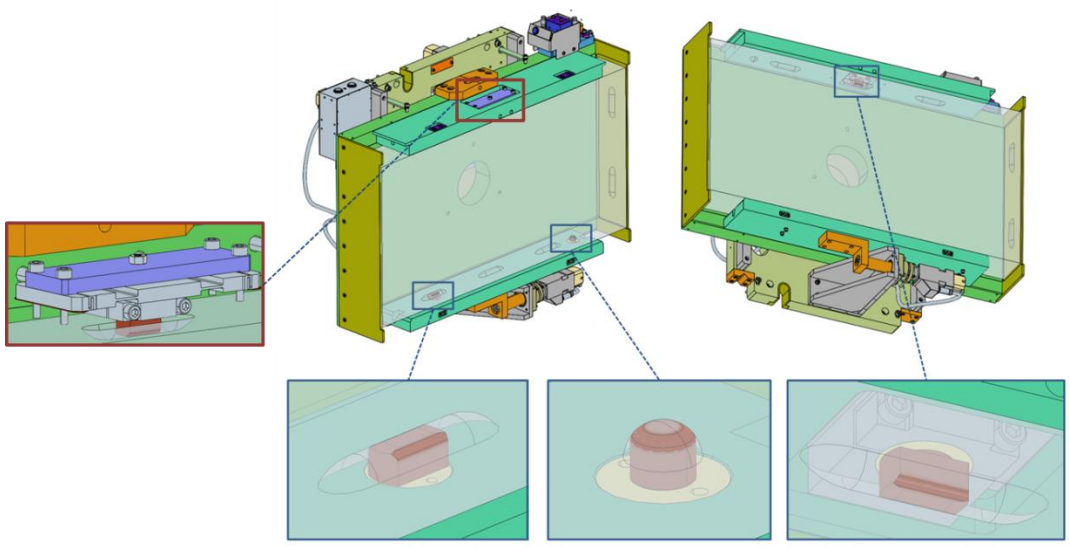

Figure 6 – Grating LRU Optic Supported by Dowel Mount

The upper dowel is seated with a flexure made from hardened 13-8 stainless steel, which is shimmed into place such that the flexure deflects by a prescribed amount, gently preloading the optic and seating the upper dowel with a force of approximately 40 lbs (Figure 7).

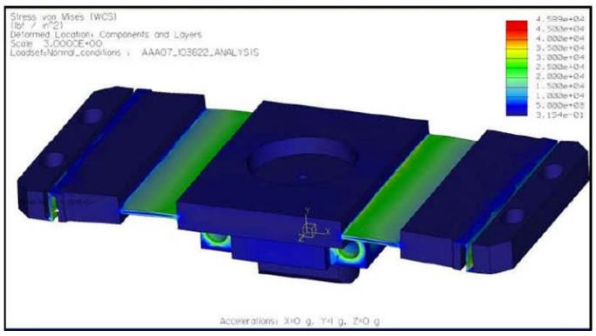

Figure 7 – Finite Element Analysis Result of Upper Dowel Flexure, Showing Deflected Shape

Early Grating LRU prototypes were assembled with dowels made from annealed 6061-T0 aluminum (Figure 11). Finite Element Analysis indicated that, under standard loading, contact with the support dowels would generate peak first-principle optic stresses of 4 MPa, which would result in a critical flaw threshold (75 MPa) margin of ~19 (Figure 8).

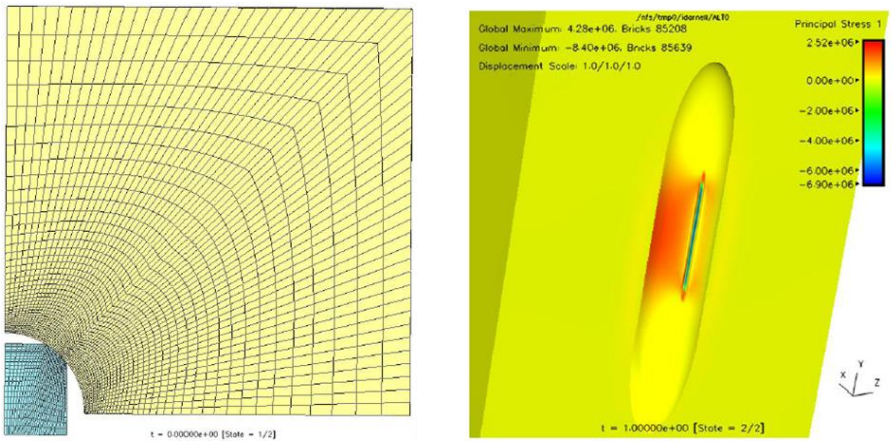

Figure 8 – Finite Element Analysis of Optic/Dowel Interface

Upon disassembling these Grating LRU prototypes, cracks were discovered at the optic/dowel interface (Figure 9). It should be noted that each Grating optic is a large, ~300 lb diffraction grating fabricated in-house at LLNL and valued at over $250,000. Operational spares are limited. Considering the significant margin indicated by contact analysis, this optic damage was unexpected. After considerable investigation and discussion with optics materials experts, it was hypothesized that these cracks developed during optic installation onto the prototype Grating LRU frame. The optic had been set on the dowel support via a compliant carriage

known as the Grating Optic Lifting Fixure (GOLF) (Figure 10). This carriage was designed to allow the optic to rock freely, aiding in seating the optic gently on the support dowels, without overloading the assembly. It was hypothesized that, as an unexpected result of this compliance, the optic experienced significant tangential (friction) contact loading as it was set onto its dowel supports. In conjunction with normal contact loading, tangential loading is known to generate significantly higher first-principle stresses than normal loading alone.

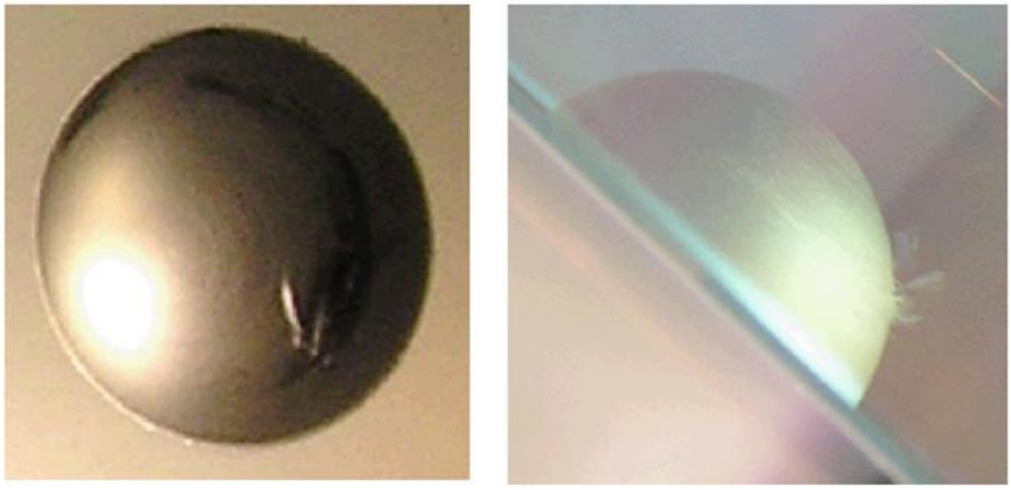

Figure 9 – Cracks in Prototype Grating LRU Optic Dowel Support Grooves

Figure 10 – Grating Optic Installation into LRU Frame Using the GOLF

In response to this issue, the optic support dowels were redesigned. After considering a number of potential solutions, it was determined that the new optic support features should retain their original physical dimensions, but feature Vespel caps which, while offering acceptable robustness when exposed to ARC beampath hazards such as high-power laser light and neutron radiation, would provide a more compliant, lower friction optic contact surface (Figure 11). These new dowels were fabricated and a cold flow test was performed on an Instron test machine to verify the dowels were geometrically stable when subject to loads equivalent to that of the Grating optic. After the dowels showed no signs of cold flow, a Grating LRU frame was assembled with these new features. A Grating optic was installed, and the LRU packaged and transported around the NIF facility to simulate dynamic loads typical when LRUs are shipped from our in-house cleanroom assembly building to the NIF Target Bay for installation in the ARC beampath. After completion of this test, no optic cracking was observed, and Grating LRU production continued. An additional 16 Grating LRUs have since

been assembled, none of which have exhibited any optic damage due to the re-designed dowel mounts. An analysis of the Optic-Edge Dowel Support System is presented in Appendix A.

Figure 11 – Original Annealed Aluminum Dowels (Above), and Redesigned Dowels with Vespel Caps (Below)

Actuated Flexure System

In order to provide rigid restraint of the Grating LRU optic while allowing for rotational adjustment, the LRU incorporates an actuated flexure system. The Grating LRU optic frame is mounted to its actuator plate by means of 6 flexures (Figure 12). Each flexure is made from 13-8 stainless steel, hardened to 210,000 psi yield strength. Additionally, each flexure has thin blade features, machined by wire EDM, that allow the flexure to bend in manner that allows for compliance in all degrees of freedom except the direction along the flexure primary axis (Figure 13). Together, the 6 flexures constrain the optic and its frame in six degrees of freedom, which provide for a rigid mount without over-constraint.

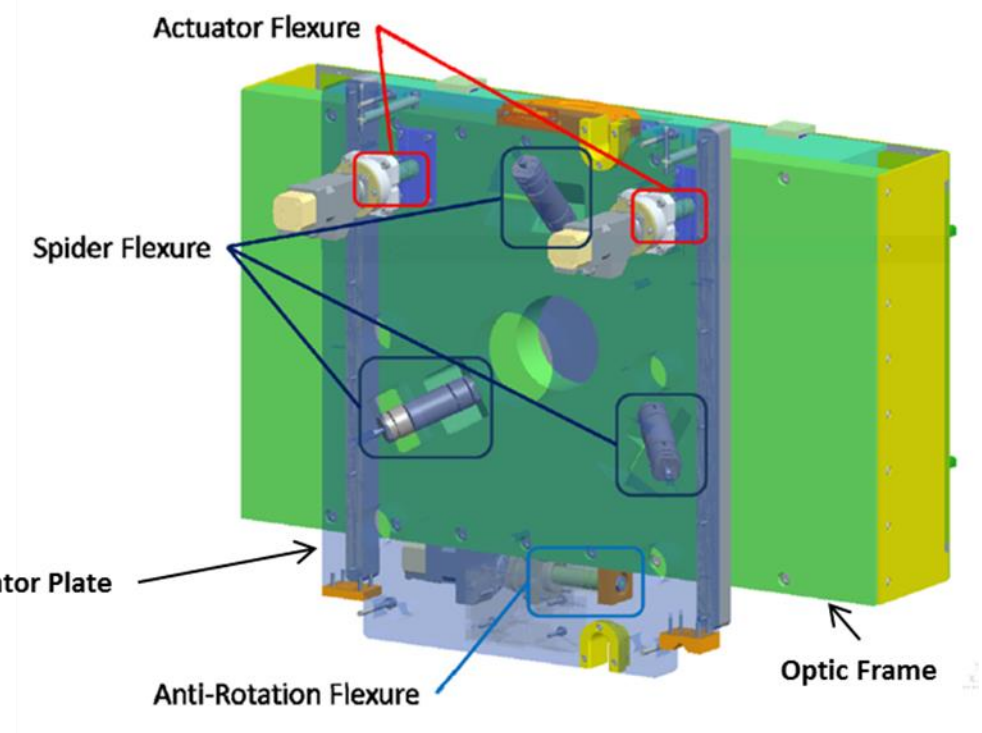

Figure 12 – Grating LRU Flexure System – Note the Actuator and Anti-Rotation Flexures are Mounted to Motorized Actuators

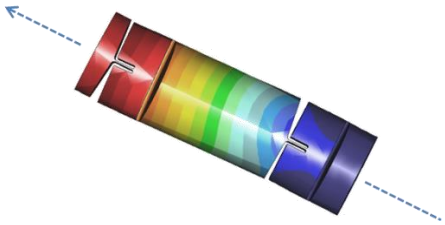

Figure 13 – Finite Element Model of an Individual Flexure, Showing Typical Deflection and Flexure Primary Axis

The actuator flexures and anti-rotation flexure are mounted to motorized actuators, which, when driven, allow the Grating LRU optic to be adjusted in rotation about three axes. These rotations are commonly referred to as tip, tilt, and rotation. The three large central flexures, known as spider flexures, together create a point at which the optic is constrained and cannot move. This point is called the center of rotation and is intentionally located near the center of the front face of the Grating LRU optic (Figure 14). A detailed finite element analysis

model has been created to determine stresses and deflections in the LRU flexure system. This model is presented in Appendix B.

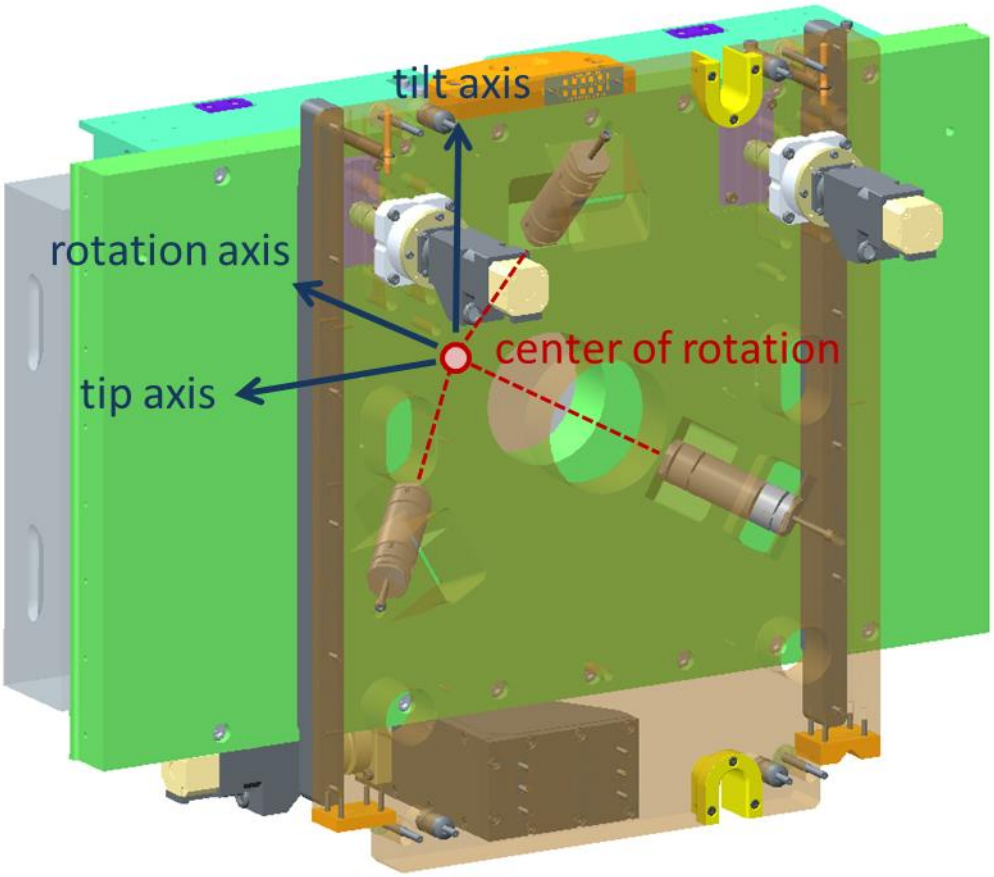

Figure 14 – Grating LRU Adjustable Degrees of Freedom

Piston Adjustment Mount

Each Grating LRU is mounted in the ARC beampath by means of a kinematic vee and flat (Figure 15), as well as 4 Harbinger micro-positioners, also called micposis (Figures 16 and 17). The kinematic vee and flat each engage kinematic pins, locating the Grating LRU in the x and y-directions according to the coordinate system shown in Figure 15. This kinematic connection allows for repeatable and tightly-toleranced positioning of the Grating LRU through multiple installation and removal cycles. The Harbinger micposis can be threaded in and out of tapped holes in the Grating LRU actuator plate and each locked in place with a fastener that registers in a counterbored hole running down the center of the micpsoi and threading into a receiver in the Grating LRU mount. The mount end of the micro-positioner is convex and the receiver

concave, which allows the mount to properly seat despite any small machine tolerance errors that might exist between various features. A detailed analysis of the Piston Adjustment Mount is presented in Appendix C.

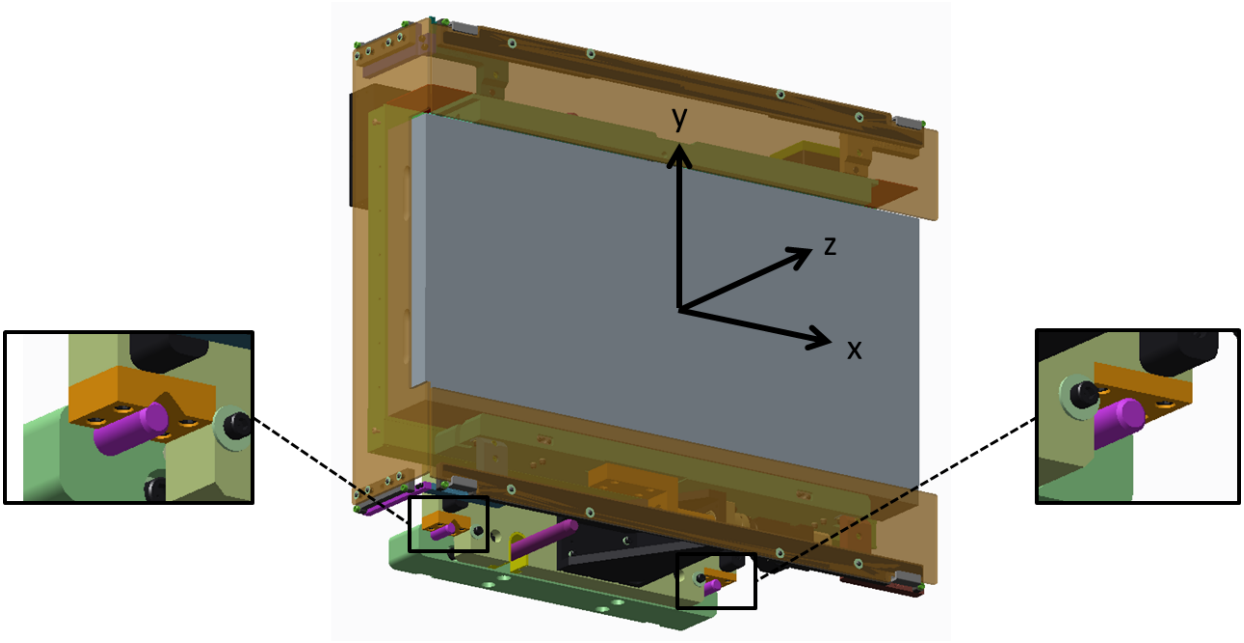

Figure 15 – Grating LRU with Kinematic Vee and Flat Registering on Precision Pins

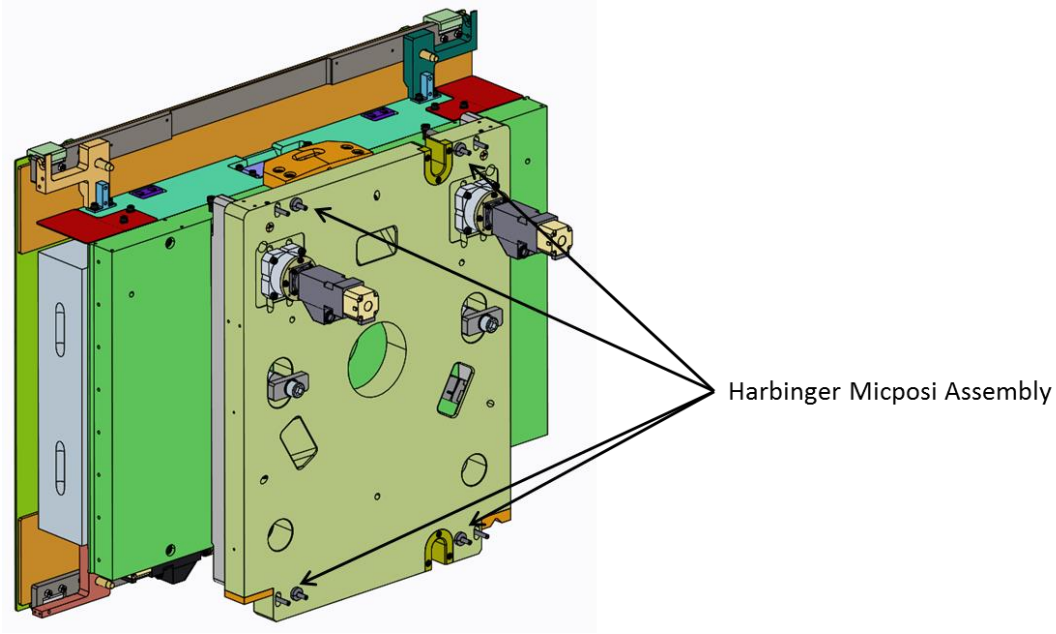

Figure 16 – Location of Qty. 4 Harbinger Micposi Assemblies

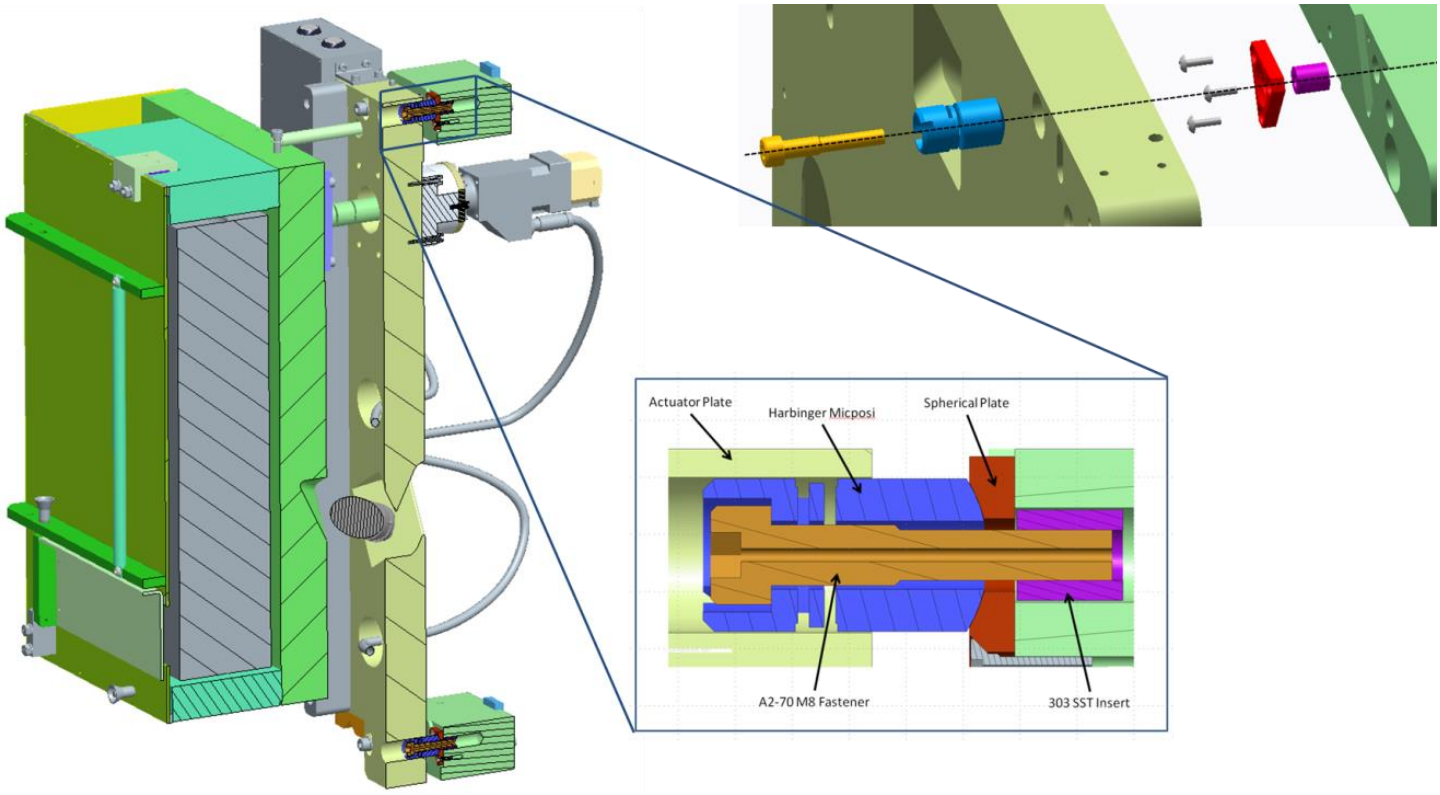

Figure 17 – Cross-Section and Exploded Views of Harbinger Micposi Assembly

Secondary Restraint System

Driving the Grating LRU actuators to extreme travel configurations can result in significant deflection of and stresses in the flexure support system. Although the flexures were designed to provide adequate safety margin under all actuator configurations such that failure of the system should never occur, it was considered prudent to implement a secondary restraint system. This system provides a means of capture of the Grating LRU optic and surrounding optic frame by utilizing posts that mount to the back of the optic frame and extend through holes in the actuator plate. The Grating LRU optic frame with posts was modeled in finite element software to verify adequate clearance with the holes in the actuator plate through the entire range of travel. These posts feature an outer flange that functions as a tether in the event of flexure failure. Additionally, the lower anti-rotation flexure bracket is designed to function as a ledge supporting the vertical weight of the optic assembly in the event of flexure failure (Figure 18).

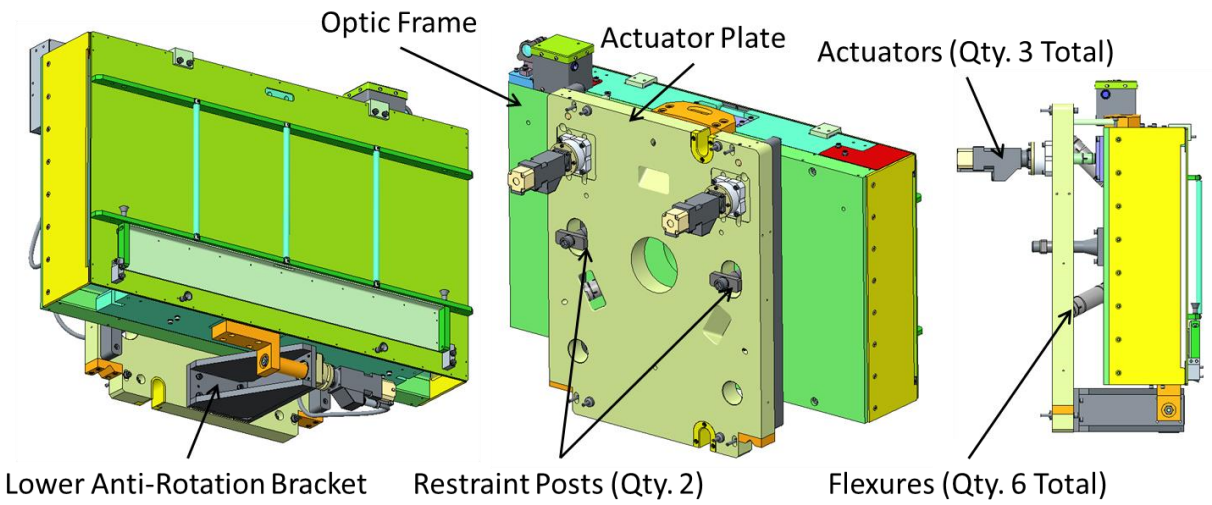

Figure 18 – Grating LRU Secondary Restraint System

The secondary restraint posts are designed with a tapered cross-section which allows for a more uniform bending stress distribution of the restraint when modeled as a cantilever beam. Additionally, the restraints are 304 stainless steel, which offers significantly greater ductility and ultimate strength when compared to alternative materials such as 6061-T6 aluminum. The secondary restraint posts feature a removable flanged cap, which mounts to the post with one M16 fastener. This cap must be removable to allow for assembly of the secondary restraint onto the Grating LRU. A detailed analysis of the Secondary Restraint System is presented in Appendix D.

Ghost-Mitigation Armor Glass

Stray light in the ARC beampath may be sufficiently powerful to damage exposed materials. When struck with laser light, metals, plastics, and other materials may ablate particles outward. These ejecta pose a hazard to the ARC system optics, as they may deposit on optical surfaces, impacting laser performance. In order to mitigate this hazard, absorbing glass has been installed in various places in the ARC beampath. This absorbing glass, similar to tinted window glass, absorbs stray laser light and safely dissipates its energy, acting as “armor” for the materials it shadows.

Unfortunately, due to scheduling demands, stray laser light threats to the Grating LRUs were not fully appreciated until after these LRUs were installed and aligned in the ARC beampath. Therefore, the ARC team was tasked with designing armor glass that could be readily installed on Grating LRUs in-situ, without significant risk to optics and without impacting Grating alignment. The design team's solution is described subsequently.

First, transport and handling (T&H) covers are installed on a Grating LRU. These covers protect the Grating LRU optics, which feature delicate coatings which are highly susceptible to scratch damage. The T&H covers are also used when transporting the Grating LRUs between facilities and were designed and fabricated prior to the design of the ghost-mitigation armor glass. Next, qty. 4 pre-assembled brackets are installed on receivers on the Grating LRU optic frame upper and lower bars. Where possible, these brackets feature captive fasteners for ease of assembly (Figure 19).

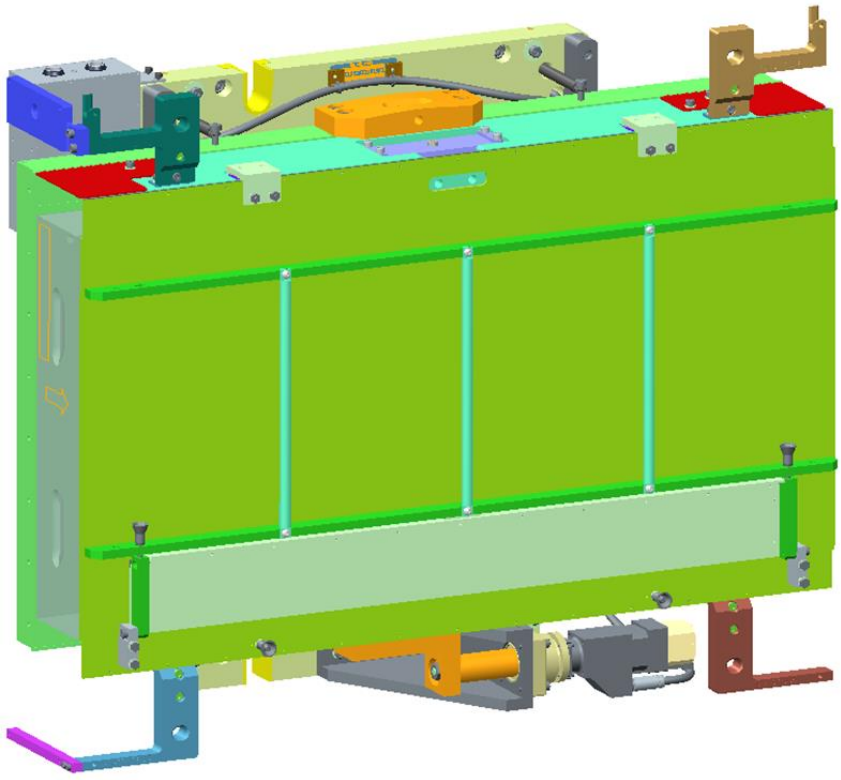

Figure 19 – Grating LRU with T&H Cover and Armor Glass Brackets Installed

Next, the T&H cover is removed, and a temporary installation cover is installed in its place (Figure 20). This installation cover is specially designed to protect the Grating optic while featuring cut-outs to allow for installation of armor glass. With the installation cover in place, pre-assembled armor glass assemblies are mounted to the brackets (Figures 21 and 22). Each piece of armor glass is mounted to an aluminum backing plate by means of polyetheretherketone (PEEK) crush bushings. A fastener is assembled through each crush bushing and a small preload torque is applied to the fastener. The crush washer, in turn, compresses and acts as a spring against the fastener head. A PEEK bearing washer is placed between the glass and fastener head to provide a compliant bearing surface. The crush bushing design allows each piece of armor glass to be precisely located and restrained without experiencing significant clamping loads or point-loading, which could lead to glass chipping or cracking. The spring action of the crush washer also helps to prevent gradual fastener preload loss over time. All PEEK hardware is susceptible to damage if exposed directly to laser light, so all crush bushings are shielded with stainless steel washers.

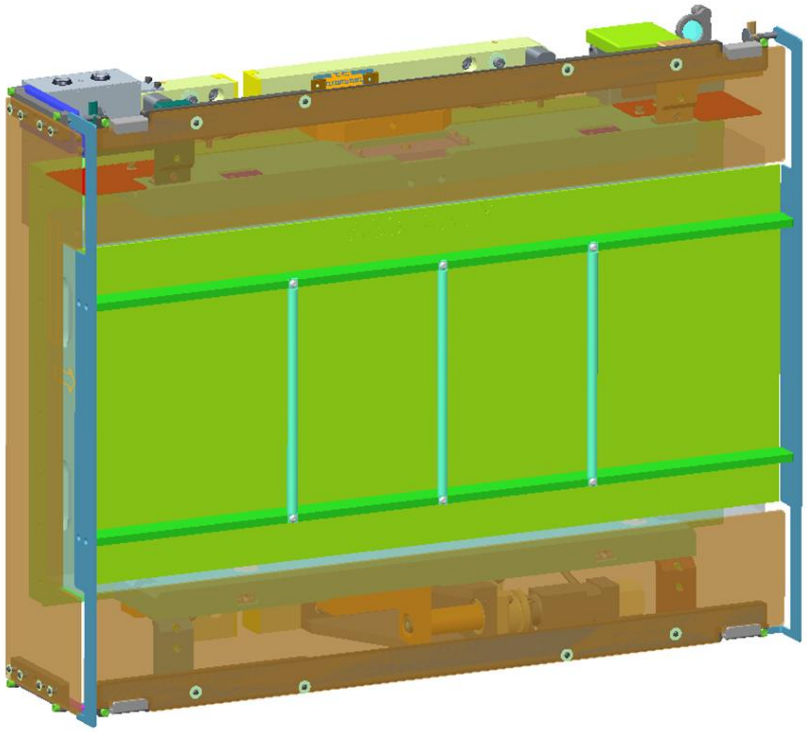

Figure 20 – Grating LRU with Temporary Installation Cover and Armor Glass Installed

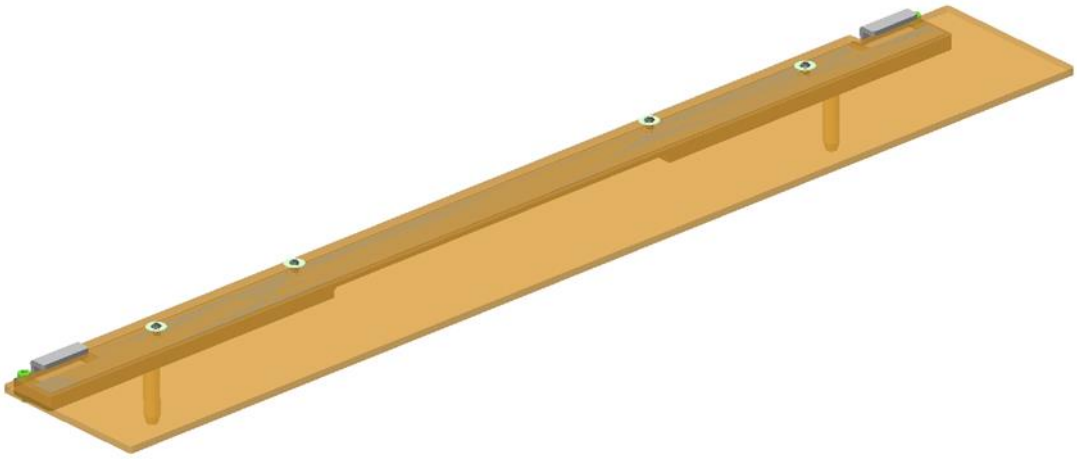

Figure 21 – Armor Glass Assembly

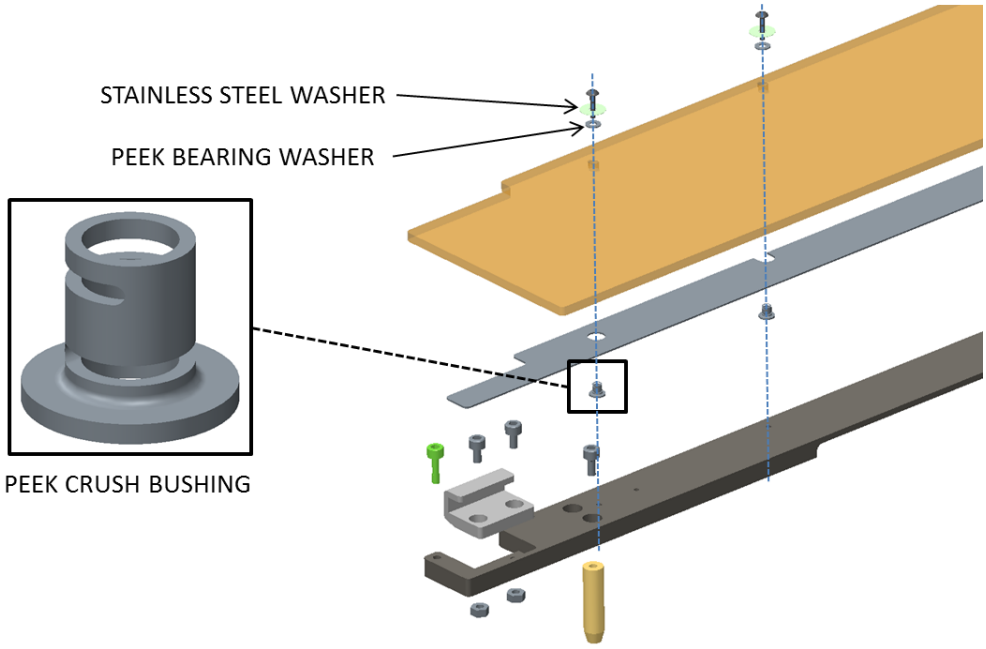

Figure 22 – Armor Glass Assembly, Exploded View

After all armor glass has been installed, the installation cover is removed and a final, operations cover is installed in its place (Figure 23). This cover protects both the Grating optic and armor glass while performing maintenance and other operations within the Compressor Vessels.

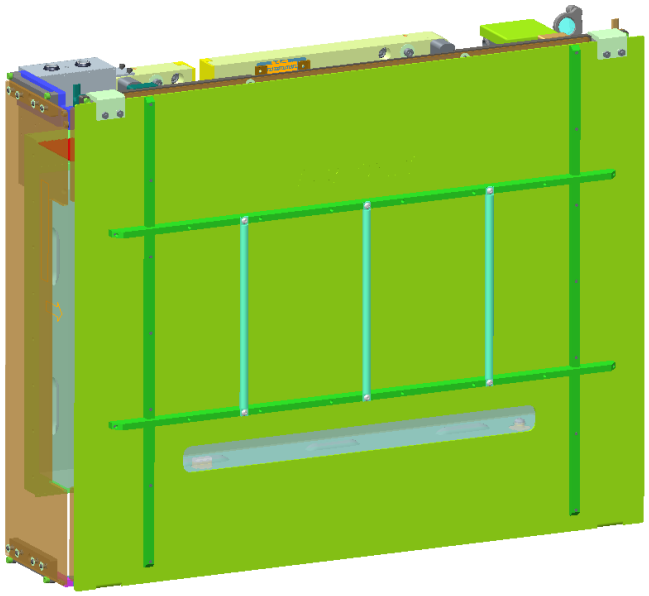

Figure 23 – Grating LRU with Operations Cover Installed

References

MESN07-500022-AB: ARC Grating LRU Assembly

NIF-0117240-AA: ARC Grating Dowel Mount Stress Memo

NIF-0117241-AA: ARC Edge Mounted Optic Stress Analysis

NIF-0114158-AA: ARC LRU Final Design Review

NIF-0118044-AA: ARC LRU Vacuum Beampath Infrastructure Final Design Review – Session #1: LRU Stability & Structural Supports

Appendix A – Optic-Edge Dowel Support Design Calculations

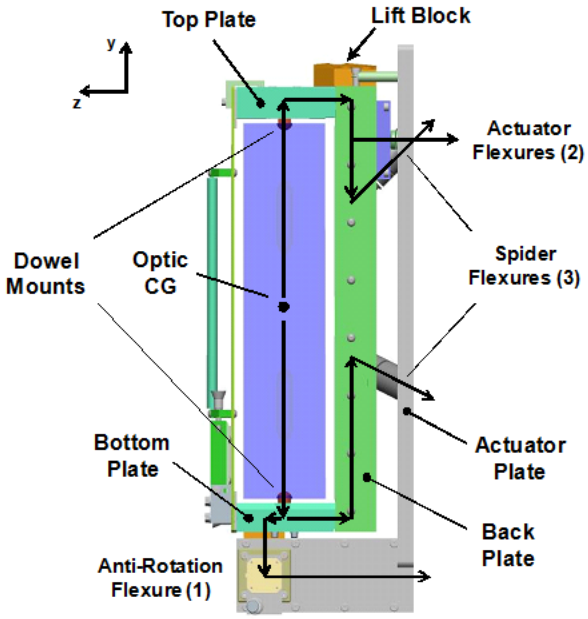

Figure A1 - Grating Optic Support Frame Components and Load Path

General Purpose and Seismic Loading

Seismic acceleration values used to analyze the Grating LRUs were obtained from in-structure response spectra of the ARC vacuum beampath. Local ARC response spectra curves were created using the NIF Target Bay and Switchyard model. The maximum individual accelerations in NIF Global x, y and z were independently selected from all four (4) grating LRU locations in the Compressor Vessels on the 29'6" level of the Target Bay. All three local peak accelerations exist at the AG1 location, but have been applied to the largest Grating LRU (AG2). The resulting seismic demand values are listed below for all three directions. The local coordinate system in which the accelerations were applied to the LRU is shown in Figure A2.

$a_{sx} := 1.62$	Horizontal (in-plane) seismic acceleration
$a_{sy} := 2.76$	Vertical seismic acceleration
$a_{sz} := 2.73$	Horizontal (optic face-normal) seismic acceleration

For calculation of general purpose safety factors, T&H loading was considered, with the dead load applied vertically down, and 0.5g applied in the most vulnerable lateral direction (either x or z). Note: the most vulnerable lateral direction is dependent on the component analyzed. Certain components may be most vulnerable when subject to an x-direction lateral load, where others may be most vulnerable to a z-direction lateral load.

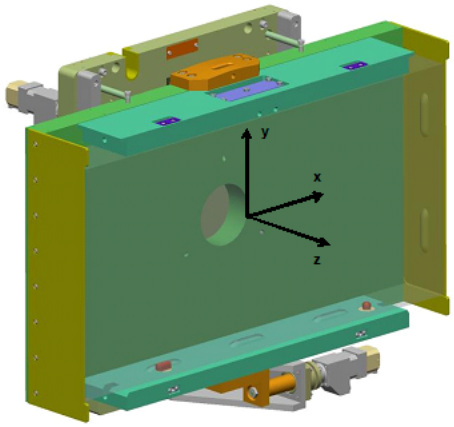

Figure A2 - Grating LRU Local Coordinate System

1. Grating Optic

While eight unique grating optics exist in the ARC compressor system, there are only two different substrate sizes, as mentioned above. Gratings number 1 and 4 are 85cm long and grating number 2 and 3 are 91cm long.

The longest grating optic substrate is used in AG2 and AG3. This is naturally the heaviest optic. Therefore, it is used for analysis of the grating LRU optic mount frame.

Dead Load

$W_{opt} := 229 \cdot lbf$ AG2 and AG3 optic weight

Seismic Forces

$F_{opt.s.x} := a_{sx} \cdot W_{opt} = 370.98\,lbf$

$F_{opt.s.y} := a_{sy} \cdot W_{opt} = 632.04\,lbf$

$F_{opt.s.z} := a_{sz} \cdot W_{opt} = 625.17\,lbf$

An analysis of the optic interaction with the dowel mounts was completed separately for the purpose of evaluating optic contact stresses at the dowel interface. It was determined that crack propagation and catastrophic failure is not a concern.

2. Spherical and Pin Dowel Mounts

The optic dowel mounts are analyzed here for structural adequacy. Both lower mounts are press-fit assemblies made of a Vespel cap pressed onto a stainless steel post.

A top level free body diagram, Figure A3, shows the combined loads generated under gravity and seismic accelerations. The reactions shown exist at the interface between the optic grooves and the dowel mounts. Reactions that result from in-plane acceleration of the optic are shown in the free body diagram in Figure A4.

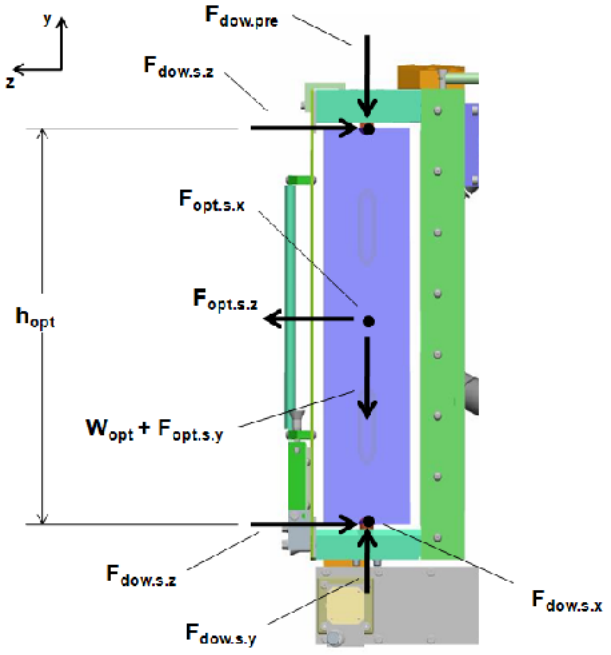

Figure A3 - Grating Optic Free Body Diagram (y-z Plane)

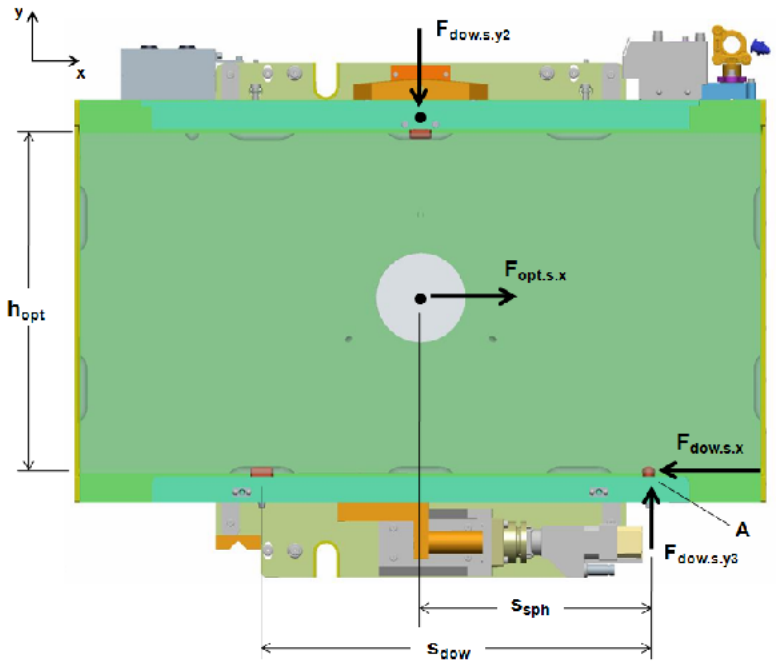

Figure A4 - Grating Optic Free Body Diagram (x-y Plane)

Dimensions

$h_{opt} := 455 \cdot mm = 17.91\,in$ $s_{sph} := 305.55 \cdot mm = 12.03\,in$ $s_{dow} := 518.05 \cdot mm = 20.4\,in$

Mount Reactions

The mount reactions shown in the previous free body diagrams, Figure A3 and Figure A4, are resolved below. The combined reactions of the bottom mounts, one pin and one spherical dowel, are first calculated. A load sharing factor is then applied based on the asymmetric mount geometry.

During LRU assembly, the upper dowel is lightly preloaded by the dowel flexure to seat the optic in the mount frame. A locking screw is then adjusted against the dowel to prevent uplift of the optic during transport and handling. By design, the dowel preload is preset and approximated to be as follows.

$F_{dow.pre} := 37.5 \cdot lbf$

Equilibrium Equations

From Figure A3:

$\Sigma F_y = F_{dow.s.y} - W_{opt} - F_{opt.s.y} - F_{dow.pre} = 0$

$F_{dow.s.y} := W_{opt} + F_{dow.pre} + F_{opt.s.y} = 898.54\,lbf$ Total force applied to lower spherical and pin dowels combined.

$\Sigma F_z = F_{opt.s.z} - 2F_{dow.s.z} = 0$

$F_{dow.s.z} := \frac{F_{opt.s.z}}{2} = 312.58\,lbf$ By symmetry, lateral load split between upper and lower dowels.

From Figure A4:

$\Sigma M_{z.A} = (F_{dow.s.y2})(s_{sph}) - (F_{opt.s.x})(h_{opt}/2) = 0$

$F_{dow.s.y2} := \frac{F_{opt.s.x} \cdot h_{opt}}{2 s_{sph}} = 276.22\,lbf$

$\Sigma F_x = F_{opt.s.x} - F_{dow.s.x} = 0$

$F_{dow.s.x} := F_{opt.s.x} = 370.98\,lbf$

$\Sigma F_y = -F_{dow.s.y2} + F_{dow.s.y3} = 0$

$F_{dow.s.y3} := F_{dow.s.y2} = 276.22\,lbf$

The forces applied through the bottom of the optic are shared by the lower spherical and pin dowel mounts. The vertical (y) and horizontal (z, normal to the optic face) forces shown in Figure A3 are slightly different between the two dowel mounts given the asymmetry about the optic center. The difference is approximated as follows, with the spherical dowel reaction factor being slightly lower than that of the pin dowel.

$C_{sph} := \frac{s_{dow} - s_{sph}}{s_{dow}} = 0.41$ $C_{pin} := \frac{s_{sph}}{s_{dow}} = 0.59$

The combined horizontal forces and total vertical forces are calculated below for the spherical and pin dowels based on the shared reaction factors.

Spherical Dowel Reactions

$F_{sph.s.shr} := \sqrt{F_{dow.s.x}^{2} + \left(C_{sph} \cdot F_{dow.s.z}\right)^{2}} = 392.51\,lbf$ Combined shear

$F_{sph.s.comp} := C_{sph} \cdot F_{dow.s.y} + F_{dow.s.y3} = 644.79\,lbf$ Compression

Lower Pin Dowel Reactions

$F_{pin.s.shr} := C_{pin} \cdot F_{dow.s.z} = 184.37\,lbf$ Shear

$F_{pin.s.comp} := C_{pin} \cdot F_{dow.s.y} + F_{dow.s.y3} \cdot \left(\frac{C_{pin}}{C_{sph}}\right) = 927.13\,lbf$ Compression

Accounting for the shared load factors, it is determined above that the spherical dowel carries a larger shear load and the pin dowel carries a larger compression load. To be conservative, consider the largest shear and compression loads applied to the spherical dowel, since it has the smallest cross-sectional area. Refer to Figure A5.

The upper dowel reactions are calculated here for the case of lateral (x and z-directions) and vertically downward applied seismic accelerations.

Upper Pin Dowel Reactions

$F_{pinu.s.shr} := F_{dow.s.z} = 312.58\,lbf$ Shear

$F_{pinu.s.comp} := F_{dow.pre} + F_{dow.s.y2} = 313.72\,lbf$ Compression

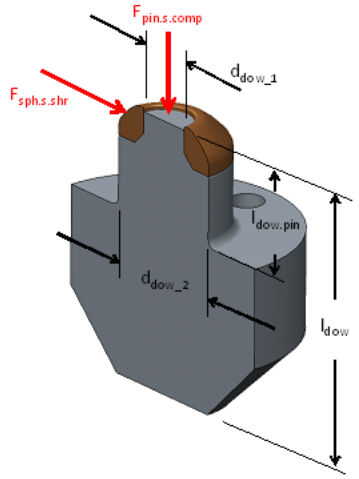

Figure A5 - Spherical Dowel Mount Dimensions (AAA12-119468) and Applied Forces

All dowel Vespel caps are fully captured between their optic grooves and dowel posts. Therefore, they are considered safe by inspection. Note that even in the worst-case situation where the Vespel caps were to yield when subject to significant external loading, the optic remains captured on the stainless steel dowel posts.

For analysis of the stainless steel post, consider two critical cross-sections:

1. The upper dowel cross-section, defined by d_{dow_1}. This cross-section is subject to shear loading only.

2. The lower dowel cross-section, defined by d_{dow_2}. This cross-section is subject to compression, shear, and bending loading.

The worst-case resulting stress will be considered for cross-sections 1 and 2, and used to compute a governing safety factor for the dowel assemblies.

Spherical Dowel Properties

$d_{dow\_1} := 7 \cdot mm = 0.28 \cdot in$ Dowel top diameter

$d_{dow\_2} := 15.53 \cdot mm = 0.61 \cdot in$ Dowel middle diameter

$A_{dow.upper} := \frac{\pi \cdot d_{dow\_1}^{2}}{4} = 0.06 \cdot in^{2}$ Dowel top cross section area

$A_{dow.lower} := \frac{\pi \cdot d_{dow\_2}^{2}}{4} = 0.29 \cdot in^{2}$ Dowel lower cross section area

$I_{dow.lower} := \frac{\pi}{4} \cdot \left(\frac{d_{dow\_2}}{2} \right)^{4} = 6.86 \times 10^{-3} \cdot in^{4}$ Dowel lower cross section area moment of inertia

$l_{dow.pin} := 12.69mm = 0.5 \cdot in$ Dowel post length

$l_{dow} := 32.69 \cdot mm = 1.29 \cdot in$ Dowel assy length (including cup)

$\sigma_{SST304.y} := 30 \cdot ksi$ Yield strength of annealed 304 stainless steel

Spherical Dowel (Upper Cross-Section) Stresses - Seismic

$$\tau_{s.upper} := \frac{\max\left(F_{sph.s.shr}, F_{pin.s.shr}\right)}{A_{dow.upper}} = 6.58 \times 10^{3}\,psi$$

Shear Stress at Dowel Upper Cross Section, Seismic, Assumes Worst-Case Shear Dowel Load

$$\sigma_{vm.s.upper} := \sqrt{3 \cdot \tau_{s.upper}^{2}} = 11.4 \cdot ksi$$

Von Mises Stress at Dowel Upper Cross Section, Seismic

Spherical Dowel (Upper Cross-Section) Stresses - General Purpose

The general purpose stresses are approximated below for 1g vertical and 0.5g horizontal acceleration (x-direction) that may be experienced during transport and handling. Refer to Figure A4.

$$\tau_{upper} := \frac{0.5 W_{opt}}{A_{dow.upper}} = 1.92 \times 10^{3}\,psi$$

T&H Load Shear Stress at Dowel Upper Cross Section (Only Spherical Dowel Reacts X-Direction Load)

$$\sigma_{vm.upper} := \sqrt{3 \cdot \tau_{upper}^{2}} = 3.32 \cdot ksi$$

T&H Load Von Mises Stress at Dowel Upper Cross Section

Spherical Dowel (Lower Cross-Section) Stresses - Seismic

$$\sigma_{s.comp} := \frac{\max\left(F_{pin.s.comp}, F_{sph.s.comp}\right)}{A_{dow.lower}} = 3.16 \cdot ksi$$

Compressive Stress at Dowel Lower Cross Section, Seismic, Assumes Worst-Case Compressive Dowel Load

$$\tau_{s.lower} := \frac{\max\left(F_{pin.s.shr}, F_{sph.s.shr}\right)}{A_{dow.lower}} = 1.34 \times 10^{3}\,psi$$

Shear Stress at Dowel Lower Cross Section, Seismic, Assumes Worst-Case Shear Dowel Load

$$\sigma_{s.bend} := \frac{\max\left(F_{pin.s.shr}, F_{sph.s.shr}\right) \cdot l_{dow.pin} \cdot \left(\frac{d_{dow\_2}}{2}\right)}{I_{dow.lower}} = 8.74 \cdot ksi$$

Bending Stress at Dowel Lower Cross Section, Seismic, Assumes Worst-Case Shear Dowel Load

$$\sigma_{vm.s.lower} := \sqrt{\left(\sigma_{s.comp} + \sigma_{s.bend}\right)^{2} + 3 \cdot \tau_{s.lower}^{2}}$$

$$\sigma_{vm.s.lower} = 12.12 \cdot ksi$$

Von Mises Stress at Dowel Lower Cross-Section, Seismic

Spherical Dowel (Lower Cross-Section) Stresses - General Purpose

The general purpose stresses are approximated below for 1g vertical and 0.5g horizontal acceleration (x-direction) that may be experienced during transport and handling. Refer to Figure A3 and A4.

$$F_{dow.y3} := \frac{0.5W_{opt} \cdot h_{opt}}{2s_{sph}}$$

General Purpose X-Direction Lateral Load on Spherical Dowel

$$\sigma_{comp} := \frac{\max\left(C_{pin}, C_{sph}\right) \cdot \left(W_{opt} + F_{dow.pre}\right)}{A_{dow.lower}} + \frac{F_{dow.y3}}{A_{dow.lower}}$$

T&H Load Compressive Stress at Dowel Lower Cross Section, Assumes Worst-Case T&H Compressive Load on Pin Dowel

$$\sigma_{comp} = 0.83 \cdot ksi$$

$$\tau_{lower} := \frac{0.5W_{opt}}{A_{dow.lower}} = 0.39 \cdot ksi$$

T&H Load Shear Stress at Dowel Lower Cross Section (Only Spherical Dowel Reacts X-Direction Load)

$$\sigma_{bend} := \frac{\left(0.5W_{opt}\right) \cdot l_{dow.pin} \cdot \left(\frac{d_{dow\_2}}{2}\right)}{I_{dow.lower}} = 2.55 \cdot ksi$$

T&H Bending Stress at Dowel Lower Cross Section, Assumes Worst-Case T&H Shear Load on Pin Dowel

$$\sigma_{vm.lower} := \sqrt{\left(\sigma_{comp} + \sigma_{bend}\right)^2 + 3 \cdot \tau_{lower}^2} = 3.44 \cdot ksi$$

Von Mises Stress at Dowel Lower Cross-Section, T&H

Next, calculate seismic and general purpose safety factors based on worst-case stresses.

$$FS_{2s} := \frac{\sigma_{SST304.y}}{\max\left(\sigma_{vm.s.upper}, \sigma_{vm.s.lower}\right)} = 2.48$$

OK - 1.0 required vs. tensile yield strength.

$$FS_2 := \frac{\sigma_{SST304.y}}{\max\left(\sigma_{vm.upper}, \sigma_{vm.lower}\right)} = 8.72$$

OK - 3.0 required vs. tensile yield strength.

Appendix B – Actuated Flexure System Finite Element Model

A Grating LRU finite element model was developed and analyzed in PTC Creo Simulate (formerly ProEngineer Mechanica). The model was based on a simplified Grating LRU solid model and featured detailed flexure geometry (Figure B1). The three spider flexures (shown below in grey) were each constrained on their outermost surfaces. The two actuator flexures and one anti-rotation flexure (shown below in green) were also constrained on their outermost surfaces, but were prescribed to set extensions along their primary axis (see arrows below). This simulated the act of actuator translation and resulted in deflections and stresses in the actuator flexure blades. Additionally, body loads were specified, simulating the effect of gravity or other static loads. Appropriate material properties were assigned to each component.

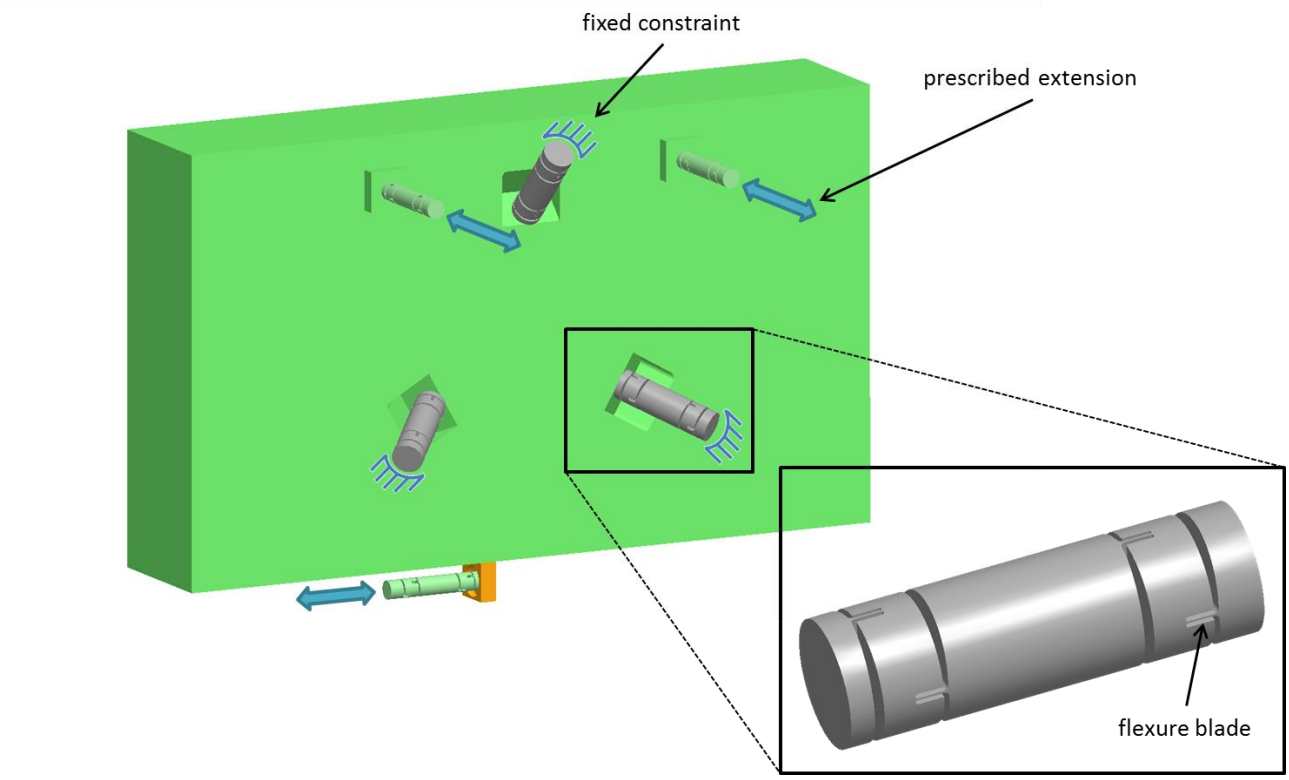

Figure B1 – Grating LRU Finite Element Model with Detailed Flexure

The model was meshed with solid tetrahedral elements utilizing an automatic meshing algorithm within the Creo software. Most cases considered only geometric linearity and perfectly elastic materials; however, a small number of case studies were performed utilizing a geometrically nonlinear solver. For most loading scenarios, the geometrically linear and nonlinear models exhibited strong correlation. Since design requirements did not allow for yielding of the flexure material, elements

featuring plasticity were not necessary; rather, all operating scenarios were required to feature resulting stresses below material yield strength. To verify model convergence, additional case studies were performed examining localized mesh refinement in areas exhibiting significant stresses. Lastly, two additional models were created, one featuring flexures with blades meshed with shell elements, and the other with blades meshed with beam elements. For most loading scenarios, deflection and stress results from these models were in general agreement with those from solid tetrahedral element model.

Results from a typical loading scenario are shown in Figure B2 and B3. Figure B2 shows the deflected model, scaled to 6x its actual deflection. Figure B3 shows the stress result in a flexure blade. Note the bending behavior of the flexure blades, apparent both in the deflected shape of the flexure, but also the stress profile of the blade. The anisotropic stiffness of an individual flexure – its ability to deform via blade bending while remaining stiff along its longest dimension, is utilized to create an optical mount that is both adjustable and avoids over-constraint.

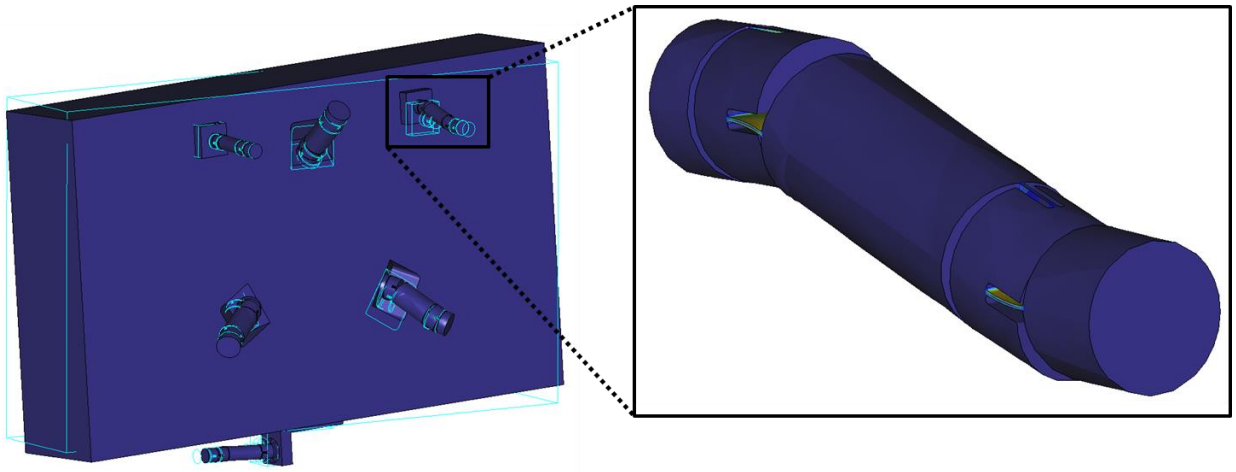

Figure B2 – Deflected Model Shape, Scaled 6x, of a Typical Finite Element Result (Undeformed Shape Shown with Light Blue Outline)

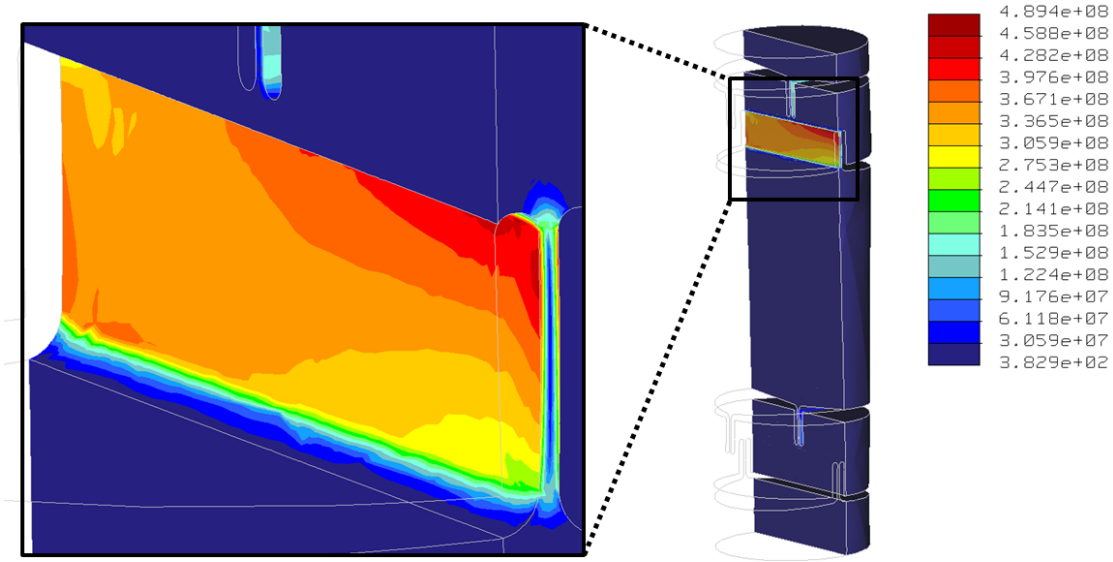

Figure B3 – Stress Profile of a Typical Finite Element Result (Units in Pa)

Appendix C – Piston Adjustment Mount Calculations

This appendix presents design calculations for certain members of the load path shown in Figure C1. The light blue arrows denote an alternate load path present during LRU installation. Unless otherwise noted, first consider seismic loading. If the resulting safety factors are less than those required for general purpose loading, additional analysis is performed. Note: for calculations considering bolt preload, a joint stiffness factor of 1 is assumed for calculations involving stresses ir the bolted connection, and a joint stiffness factor of 0 is assumed for joint separation calculations; this is conservative.

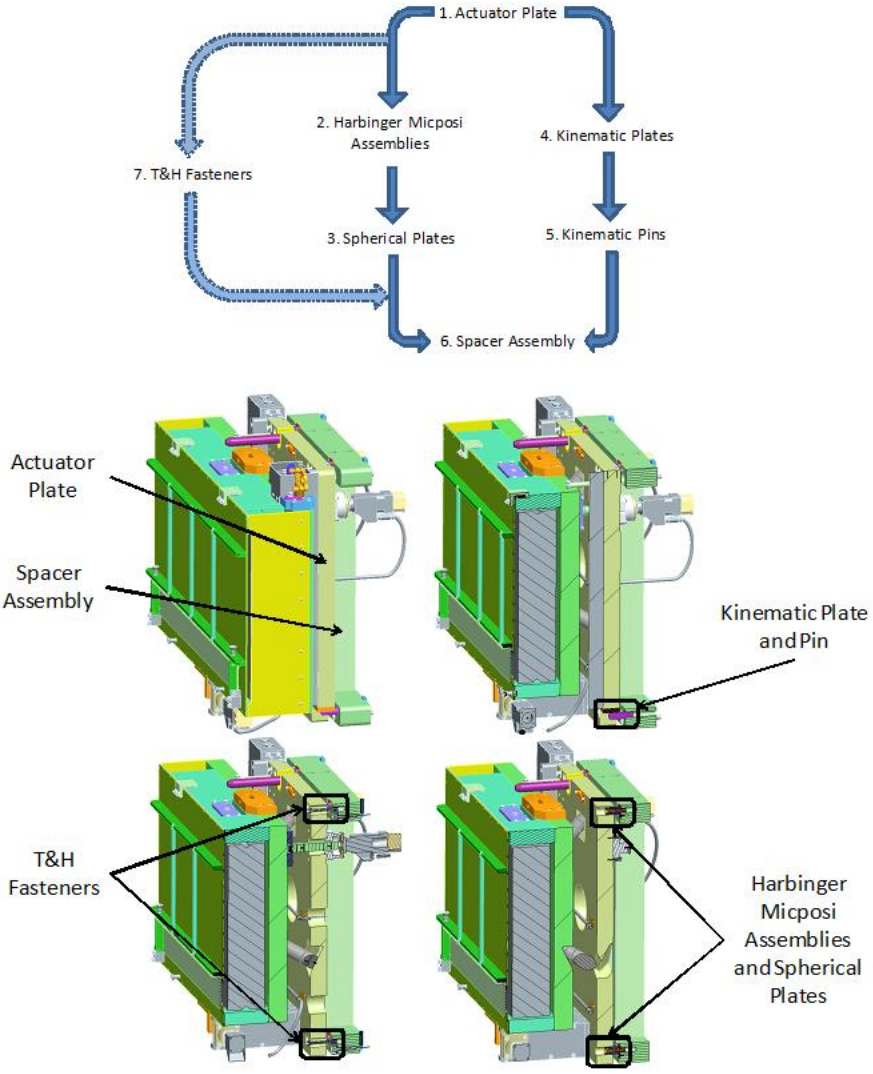

Figure C1. Load Path

1. Actuator Plate

The Harbinger Micposi Assemblies are load rated to 2120 lbf based on a 6061-T6 Aluminum Base Plate, given a minimum thread engagement of 0.22 inches on both top and bottom threaded sections. Subsequent calculations assume that all Harbinger Micposis are adjusted to maximum vendor allowable extension (with minimum thread engagement of 0.22 inches on both top and bottom thread sections). This represents the highest-stress as-installed hardware configuration.

First, reactions are determined at the blue connection points shown in Figure C2, and Actuator Plate thread shear is investigated.

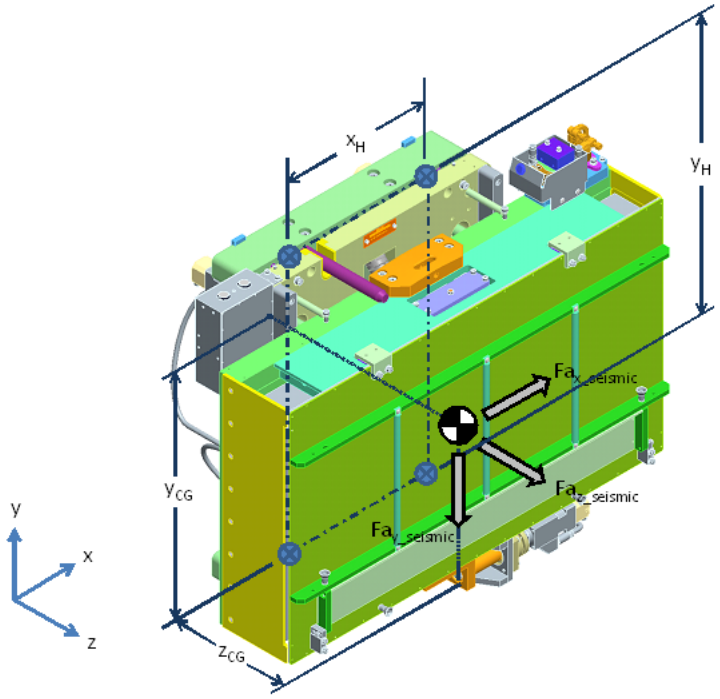

Figure C2. Seismic Loading (Connection Constraints Shown in Blue)

Consider reactions under seismic loading. Make the conservative assumption that the Harbinger Micposi assemblies support the optic load entirely; support from the kinematic pins is neglected.

$M_{AG} := 650lbm$ ARC Grating LRU mass - conservative estimate

$g = 9.807\frac{m}{s^2}$ $g = 32.174\cdot\frac{ft}{s^2}$ Gravitational acceleration

$S_x := 1.62g$ $S_y := 3.76g$ $S_z := 2.73g$ Seismic amplification factors (Sy includes 1g dead load)

$Fa_{x\_seismic} := M_{AG} \cdot S_x = 1.053 \times 10^3 \cdot lbf$

$Fa_{y\_seismic} := M_{AG} \cdot S_y = 2.444 \times 10^3 \cdot lbf$

$Fa_{z\_seismic} := M_{AG} \cdot S_z = 1.774 \times 10^3 \cdot lbf$

$z_{CG} := 200mm = 7.874 \cdot in$ Conservative estimate

$x_H := 338mm = 13.307 \cdot in$

$y_H := 640mm = 25.197 \cdot in$

The AG LRU center of gravity (CG) is approximately centered in the 4 Harbinger Micposi pattern in x and y directions. Therefore, assume the AG LRU CG is centered with respect to the Harbinger pattern in x and y directions.

Consider the x-direction applied seismic load. Assume all four Harbingers react shear equally.

$V_{x\_seismic} := \frac{Fa_{x\_seismic}}{4} = 263.25 \cdot lbf$ Shear force due to x-dir acceleration

$F_{x\_seismic} := \frac{1}{2} \cdot \frac{Fa_{x\_seismic} \cdot z_{CG}}{x_H} = 311.538 \cdot lbf$ Axial force due to x-dir acceleration

Consider the y-direction applied seismic load. Assume all four Harbingers react shear equally.

$V_{y\_seismic} := \frac{Fa_{y\_seismic}}{4} = 611 \cdot lbf$ Shear force due to y-dir acceleration

$F_{y\_seismic} := \frac{1}{2} \cdot \frac{Fa_{y\_seismic} \cdot z_{CG}}{y_H} = 381.875 \cdot lbf$ Axial force due to y-dir acceleration

Consider the z-direction applied seismic load. Because the seismic load is assumed to be centered with respect to the Harbinger pattern in x and y directions, each Harbinger reacts this load equally.

$F_{z\_seismic} := \frac{Fa_{z\_seismic}}{4} = 443.625 \cdot lbf$ Axial force due to z-dir acceleration

Therefore, the worst case axial and shear force on one Harbinger assembly is as follows:

$F_{app\_seismic} := F_{x\_seismic} + F_{y\_seismic} + F_{z\_seismic} = 1.137 \times 10^3 \cdot lbf$ Axial force

$V_{app\_seismic} := V_{x\_seismic} + V_{y\_seismic} = 874.25 \cdot lbf$ Shear force

Next, consider the effect of preload on the bolted connection.

$T := 9ft \cdot lbf$ Harbinger M8 fastener installation torque

$k := 0.2$ Friction factor - Ag-Plated SST into SST

$D_{n\_M8} := 8mm = 0.315 \cdot in$ Nominal diameter of M8 fastener

$F_o := \frac{T}{k \cdot D_{n\_M8}} = 1.715 \times 10^3 \cdot lbf$ Preload force due to M8 installation torque

Consider actuator plate thread stripping as a result of the worst case axial load (preload included).

$Le_{act\_min} := 0.22in = 5.588 \cdot mm$ Minimum actuator plate / Harbinger thread engagement on one side of flexure

$D_{Harbinger} := 22mm - 1.5mm = 20.5 \cdot mm$ Harbinger mean diameter

$D_{Harbinger} = 0.807 \cdot in$

$A_{act\_thread} := \frac{\pi \cdot D_{Harbinger} \cdot Le_{act\_min}}{2} = 179.941 \cdot mm^2$ Actuator Plate thread shear area

$A_{act\_thread} = 0.279 \cdot in^2$

$\tau_{act\_thread} := \frac{F_{app\_seismic} + F_o}{A_{act\_thread}} = 10.224 \cdot ksi$ Actuator Plate thread shear stress (assumes joint stiffness factor, C=1)

$\sigma_{yield\_6061T6} := 35ksi$ Actuator Plate tensile yield strength

$\tau_{yield\_6061T6} := \frac{1}{\sqrt{3}} \cdot \sigma_{yield\_6061T6} = 20.207 \cdot ksi$ Actuator Plate shear yield strength

$SF_{act\_thread} := \frac{\tau_{yield\_6061T6}}{\tau_{act\_thread}} = 2.0$ Actuator Plate thread shear safety factor (greater than 1.67 GPSF (General Purpose Safety Factor) and 1 RESF (Rare Event Safety Factor) requirement)

2. Harbinger Micposi Assemblies

Next, consider the reactions determined previously (Figure C2) and apply them to the Harbinger Micposi Assemblies. A margin is calculated based on a vendor provided load rating. Preload is not considered.

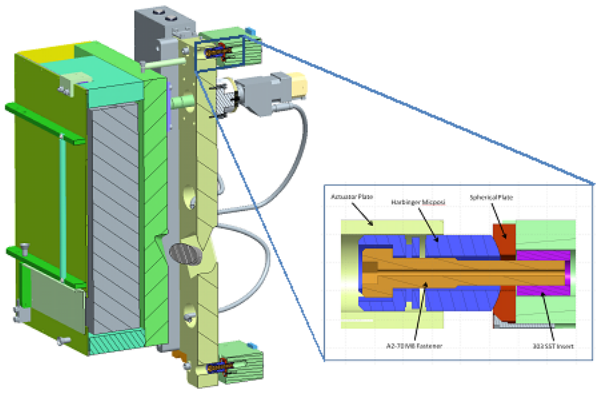

Figure C3. Harbinger Micposi Assembly

$F_{H\_max} := 2120lbf$ Manufacturer rated maximum load for Harbinger Micposi

$$SF_{Harbinger} := \frac{F_{H\_max}}{\sqrt{F_{app\_seismic}^{2} + 3 \cdot V_{app\_seismic}^{2}}} = 1.1$$

Margin against manufacturer load capacity (margin greater than 1 required, preload not considered)

The associated stresses in the M8 fasteners are as follows (preload included):

$A_{M8\_vented} := 36.6mm^{2} - 2.46mm^{2} = 34.14 \cdot mm^{2}$ Stress area of vented M8 fastener

$A_{M8\_vented} = 0.053 \cdot in^{2}$

$$\sigma_{M8\_seismic} := \frac{F_{app\_seismic} + F_{o}}{A_{M8\_vented}} = 53.887 \cdot ksi$$

Stress in M8 fastener due to preload and applied load

$\sigma_{yield\_A270} := 65ksi$ A2-70 tensile yield strength

$$SF_{M8\_seismic} := \frac{\sigma_{yield\_A270}}{\sigma_{M8\_seismic}} = 1.2$$

M8 fastener seismic safety factor (greater than 1 RESF requirement)

Consider the M8 threads in shear (preload included).

$D_{n\_M8} = 8 \cdot mm$ M8 fastener nominal diameter

$D_{n\_M8} = 0.315 \cdot in$

$P_{M8} := 1.25mm = 0.049 \cdot in$ M8 fastener pitch

$D_{m\_M8} := D_{n\_M8} - P_{M8} = 0.266 \cdot in$ M8 fastener mean diameter

$Le_{M8} := 12.6mm = 0.496 \cdot in$ M8 fastener engagement length

$A_{M8\_thread} := \frac{\pi \cdot D_{m\_M8} \cdot Le_{M8}}{2} = 0.207 \cdot in^2$ M8 fastener thread shear area

$\tau_{M8\_thread\_seismic} := \frac{F_{app\_seismic} + F_o}{A_{M8\_thread}} = 13.771 \cdot ksi$ M8 fastener thread shear stress

$\tau_{yield\_A270} := \frac{1}{\sqrt{3}} \cdot \sigma_{yield\_A270} = 37.528 \cdot ksi$ A2-70 shear yield strength

$SF_{M8\_thread\_seismic} := \frac{\tau_{yield\_A270}}{\tau_{M8\_thread\_seismic}} = 2.7$ M8 Fastener thread safety factor (greater than 1.67 GPSF and 1 RESF requirement)

Consider the SST inserts in shear (preload included).

$\tau_{yield\_303SST} := \frac{1}{\sqrt{3}} \cdot 30ksi = 17.321 \cdot ksi$ stainless steel shear yield strength

$SF_{303insert\_seismic} := \frac{\tau_{yield\_303SST}}{\tau_{M8\_thread\_seismic}} = 1.3$ Insert shear safety factor (greater than 1 RESF requirement)

Next, consider joint separation of the Harbinger interface (preload included).

$P_o := F_o = 1.715 \times 10^3 \cdot lbf$ Load required to separate joint (assumes joint stiffness factor, C=0)

$SF_{separation\_seismic} := \frac{P_o}{F_{app\_seismic}} = 1.5$ Joint separation safety factor (greater than 1 RESF and GPSF requirement)

Consider stresses under dead loading only. Only safety factors that do not meet the general purpose safety factor (GPSF) requirement under seismic loading are recalculated. Make the conservative assumption that the Harbinger Micposi assemblies support the optic load entirely; support from the kinematic pins is neglected.

$S_{y\_static} := g = 9.807 \cdot \frac{m}{s^2}$ Dead load amplification factor

$S_{y\_static} = 32.174 \cdot \frac{ft}{s^2}$

$Fa_{y\_static} := M_{AG} \cdot S_{y\_static} = 650 \cdot lbf$

Consider the y-direction applied static load. Assume all four Harbingers react shear equally.

$V_{y\_static} := \frac{Fa_{y\_static}}{4} = 162.5 \cdot lbf$

$F_{y\_static} := \frac{1}{2} \cdot \frac{Fa_{y\_static} \cdot z_{CG}}{y_H} = 101.563 \cdot lbf$

Therefore, the worst case axial and shear force on one Harbinger assembly is as follows:

$F_{app\_static} := F_{y\_static} = 101.563 \cdot lbf$

$V_{app\_static} := V_{y\_static} = 162.5 \cdot lbf$

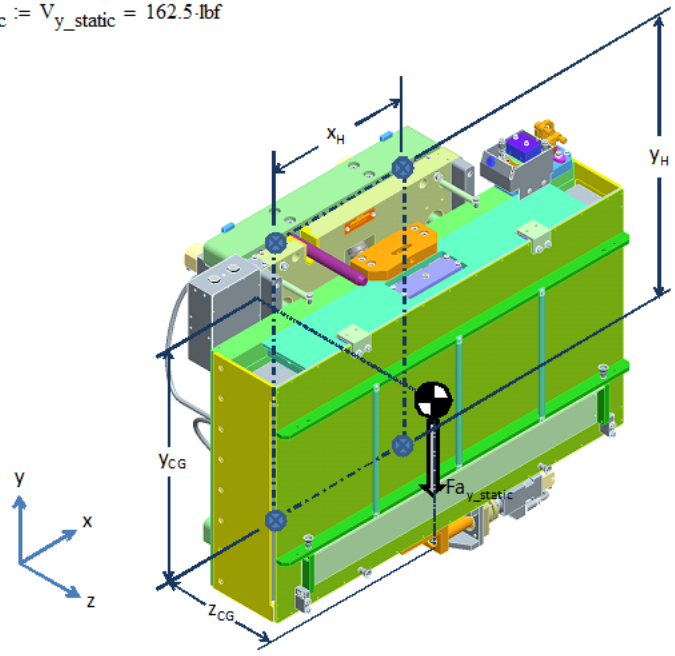

Figure C4. Static Loading (Connection Constraints Shown in Blue)

$F_{H\_max} := 2120lbf$ Manufacturer rated maximum load for Harbinger Micposi

$$SF_{Harbinger} := \frac{F_{H\_max}}{\sqrt{F_{app\_static}^{2} + 3 \cdot V_{app\_static}^{2}}} = 7.1$$

Margin against manufacturer load capacity (margin greater than 1 required, preload not considered)

The associated stresses in the M8 fasteners are as follows (preload included):

$A_{M8\_vented} := 36.6mm^{2} - 2.46mm^{2} = 34.14 \cdot mm^{2}$

$A_{M8\_vented} = 0.053 \cdot in^{2}$ Vented M8 fastener stress area

$$\sigma_{M8\_static} := \frac{F_{app\_static} + F_{o}}{A_{M8\_vented}} = 34.319 \cdot ksi$$

$\sigma_{yield\_A270} := 65ksi$ A2-70 tensile yield strength

$$SF_{M8\_GP} := \frac{\sigma_{yield\_A270}}{\sigma_{M8\_static}} = 1.9$$

M8 fastener seismic safety factor (greater than 1.33 GPSF requirement)

Consider the SST inserts in shear (preload included).

$D_{n\_M8} = 8 \cdot mm$ M8 fastener nominal diameter

$D_{n\_M8} = 0.315 \cdot in$

$P_{M8} := 1.25mm = 0.049 \cdot in$ M8 fastener pitch

$D_{m\_M8} := D_{n\_M8} - P_{M8} = 0.266 \cdot in$ M8 fastener mean diameter

$Le_{M8} := 12.6mm = 0.496 \cdot in$ M8 fastener engagement length

$$A_{M8\_thread} := \frac{\pi \cdot D_{m\_M8} \cdot Le_{M8}}{2} = 0.207 \cdot in^{2}$$

M8 fastener thread shear area

$$\tau_{M8\_thread\_static} := \frac{F_{app\_static} + F_{o}}{A_{M8\_thread}} = 8.77 \cdot ksi$$

M8 fastener thread shear stress

$$\tau_{yield\_A270} := \frac{1}{\sqrt{3}} \cdot \sigma_{yield\_A270} = 37.528 \cdot ksi$$

A2-70 shear yield strength

$$\tau_{yield\_303SST} := \frac{1}{\sqrt{3}} \cdot 30ksi = 17.321 \cdot ksi$$

stainless steel shear yield strength

$$SF_{303insert\_GP} := \frac{\tau_{yield\_303SST}}{\tau_{M8\_thread\_static}} = 2.0$$

Insert shear safety factor (greater than 1.67 GPSF requirement)

3. Spherical Plates

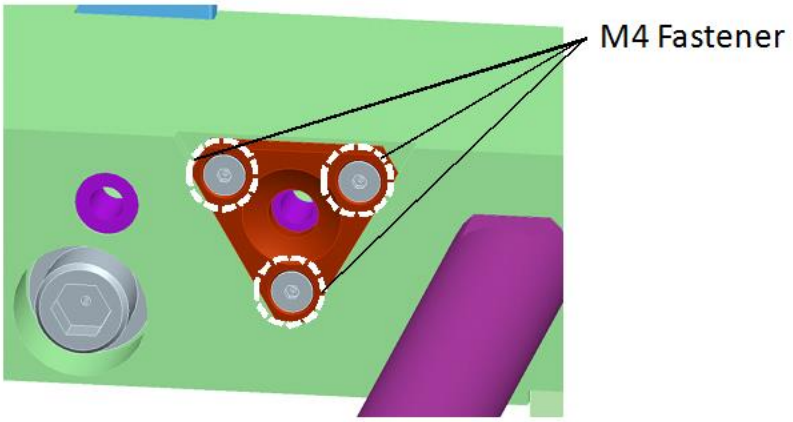

Figure C5. Spherical Plate

Because the Harbinger interface joint separation safety factor is greater than 1.0, the joint should not separate and the spherical plate M4 fasteners shown above should carry negligible shear load, as the properly preloaded joint will support the shear load. Therefore, these components are considered safe by inspection.

4. Kinematic Plate

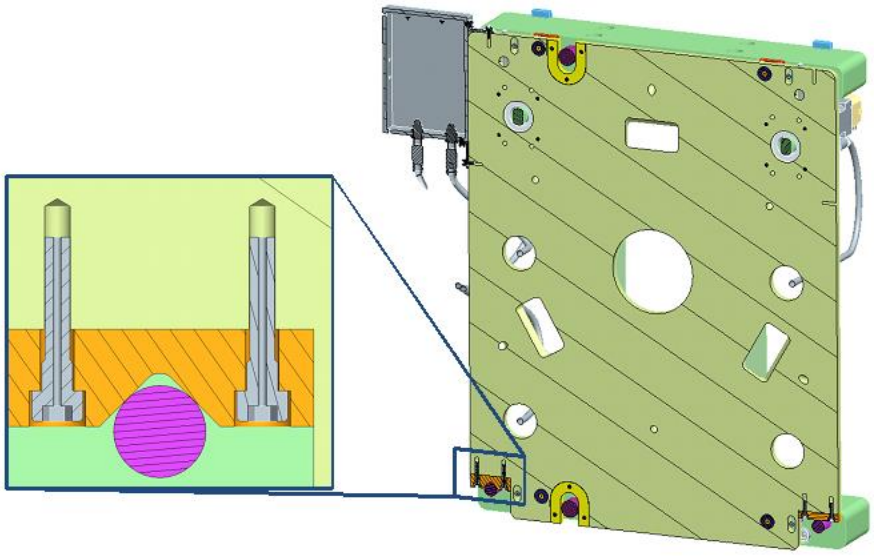

Figure C6. Kinematic Interface

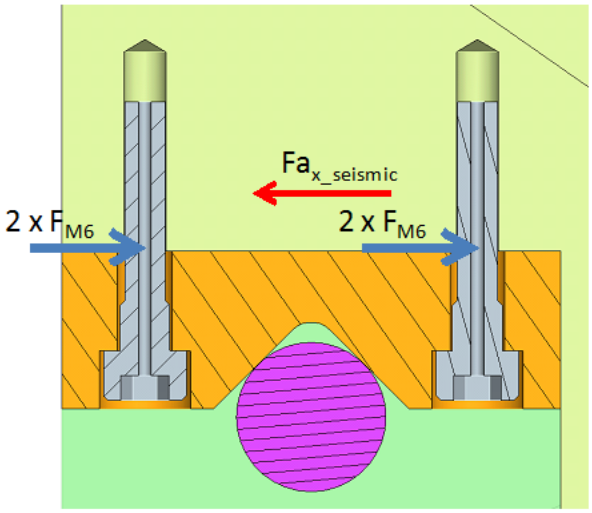

Figure C7 Kinematic Plate Fastener FBD

The kinematic plates are connected to the actuator plate via 4 vented M6 fasteners each. Assume compressive stresses are absorbed by the mated materials; consider only shear. Conservatively assume the entire x-direction seismic shear load is reacted by the v-groove block (preload not considered).

$M_{AG} = 650 \cdot lbm$ ARC Grating LRU mass - conservative estimate

$S_x = 1.62 \cdot g$ x-direction seismic acceleration

$Fa_{x\_seismic} := M_{AG} \cdot S_x = 1.053 \times 10^{3} \cdot lbf$ x-direction seismic load

$\Sigma F_x \quad F_{shear} := \frac{1}{4} \cdot Fa_{x\_seismic} = 263.25 \cdot lbf$ Shear force on M6 fastener

$Dr_{M6} := 6mm - 1.226869 \cdot 1mm = 4.773 \cdot mm$ M6 fastener root diameter

$As_{M6} := \frac{\pi \cdot Dr_{M6}^{2}}{4} - 1.94mm^{2} = 15.954 \cdot mm^{2}$ Shear stress area of kinematic v-groove plate fastener

$As_{M6} = 0.025 \cdot in^{2}$

$\tau_{M6} := \frac{F_{shear}}{As_{M6}} = 10.646 \cdot ksi$ Shear stress in vented M6 fastener

$SF_{M6} := \frac{\tau_{yield\_A270}}{\tau_{M6}} = 3.5$ M6 Fastener shear safety factor (greater than 1 RESF requirement)

5. Kinematic Pins

Assume the kinematic pins react the entire negative y-direction seismic acceleration; however, the Harbinger Micposi Assemblies react all lateral loads and restore the tipping moment resulting from negative y-direction acceleration. Neglect transverse shear stress.

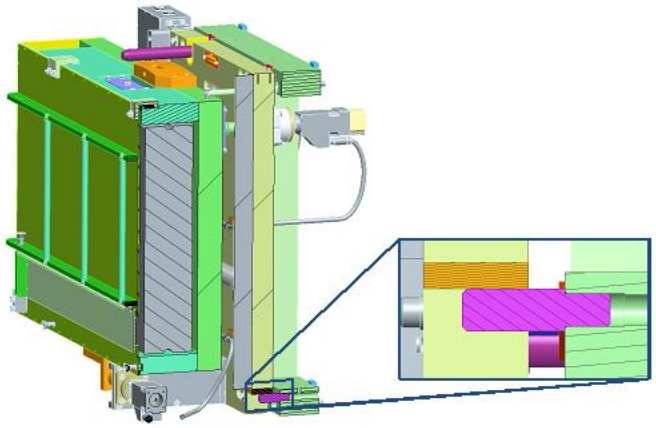

Figure C8. Kinematic Pins

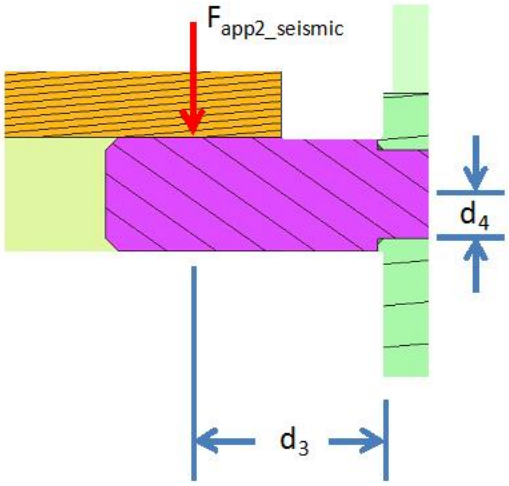

Figure C9. Kinematic Pin Beam Model

$S_{yield\_AM100} := 250ksi$ Kinematic Pin yield strength

$S_{y\_down} := 3.76g$ Seismic Amplification Factor

$F_{app2\_seismic} := M_{AG} \cdot S_{y\_down} = 2.444 \times 10^{3} \cdot lbf$ Total Force Applied to 2 Kinematic Pins

$d_3 := 28.33mm = 1.115 \cdot in$ See Figure C9

$d_4 := 7.0145mm = 0.276 \cdot in$ See Figure C9

$M_{app2} := \frac{1}{2} \cdot F_{app2\_seismic} \cdot d_3 = 1.363 \times 10^{3} \cdot lbf \cdot in$ Kinematic Pin Applied Moment

$I_{kin\_pin} := \frac{\pi}{4} \cdot d_4^{\,4} = 1.901 \times 10^{3} \cdot mm^{4}$ Kinematic Pin Second Moment of Area

$I_{kin\_pin} = 4.568 \times 10^{-3} \cdot in^{4}$

$\sigma_{kin\_pin} := \frac{M_{app2} \cdot d_4}{I_{kin\_pin}} = 82.396 \cdot ksi$ Kinematic Pin maximum bending stress

$SF_{kin\_pin} := \frac{S_{yield\_AM100}}{\sigma_{kin\_pin}} = 3.0$ Kinematic Pin safety factor (greater than 1 RESF and 3 GPSF requirement)

Appendix D – Secondary Restraint System Calculations

In this analysis, it is assumed that all flexure connections have failed. Additionally, 100% seismic loads have been applied in x, y, and z directions (coordinate system shown below). These assumptions are conservative. Additionally, the reaction load SR_1 is assumed to occur in a direction through the optic and flexure-supported frame center of mass, as shown in the figure below. The shear reaction SR_3 is assumed to be provided by one secondary restraint post only, to account for uneven load sharing.

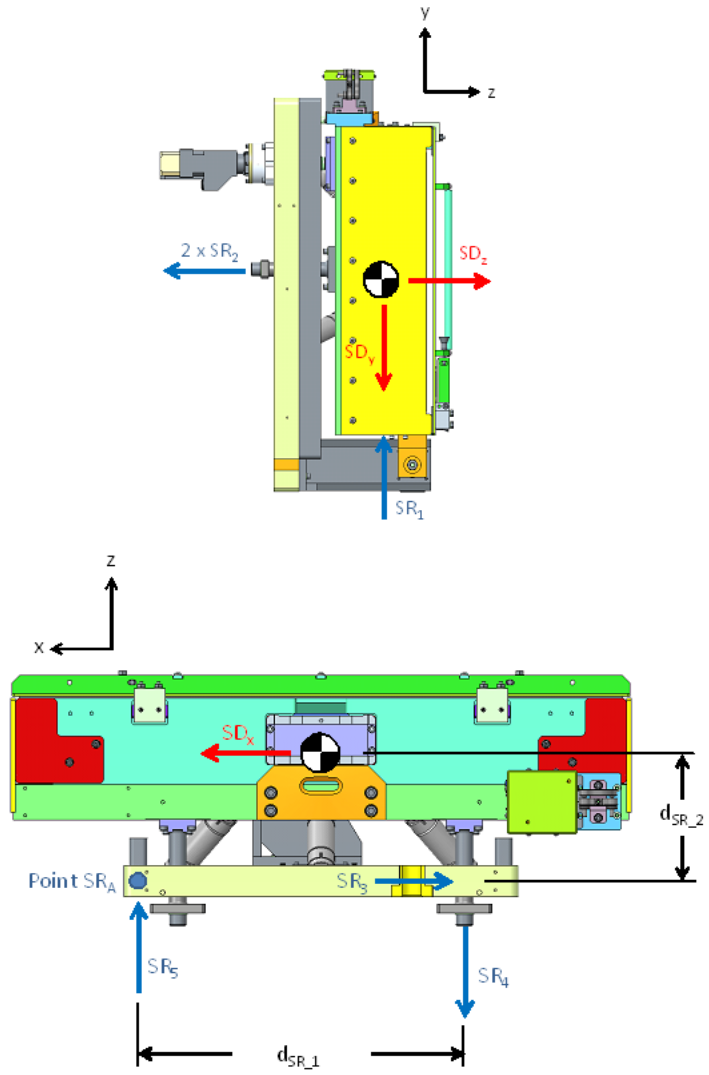

Figure D1

$W_{AG} := 480lbf$ weight of components supported by secondary restraint system (conservative estimate)

$a_x := 1.62$ $a_y := 1 + 2.76$ $a_z := 2.73$ seismic demand, y-direction includes gravity

$SD_x := a_x \cdot W_{AG} = 777.600 \cdot lbf$

$SD_y := a_y \cdot W_{AG} = 1.805 \times 10^3 \cdot lbf$

$SD_z := a_z \cdot W_{AG} = 1.310 \times 10^3 \cdot lbf$

$d_{SR\_1} := 455mm = 17.913 \cdot in$ distance from secondary restraint to stiffener rib

$d_{SR\_2} := 175mm = 6.890 \cdot in$ Creo measurement, supported weight C.G. to center of Actuator Plate (estimate)

Consider the y and z-direction seismic loads SD_y and SD_z.

$\Sigma F_y = -SD_y + SR_1 = 0$

$SR_1 := SD_y = 1.805 \times 10^3 \cdot lbf$

$\Sigma F_z = SD_z - (2 \times SR_2) = 0$

$SR_2 := \frac{SD_z}{2} = 655.200 \cdot lbf$

Consider the x-direction seismic load SD_x.

$\Sigma F_x = SD_x - SR_3 = 0$

$SR_3 := SD_x = 777.600 \cdot lbf$

$\Sigma M_{SR\_A} = (SD_x \times d_{SR\_2}) - (SR_4 \times d_{SR\_1}) = 0$

$SR_4 := \frac{SD_x \cdot d_{SR\_2}}{d_{SR\_1}} = 299.077 \cdot lbf$

$\Sigma F_z = -SR_4 + SR_5 = 0$

$SR_5 := SR_4 = 299.077 \cdot lbf$

Consider the load into the bottom anti-rotation support bracket. Consider the four fasteners mounting the bracket to the actuator plate as, by inspection, this is the weakest link in the bracket load path.

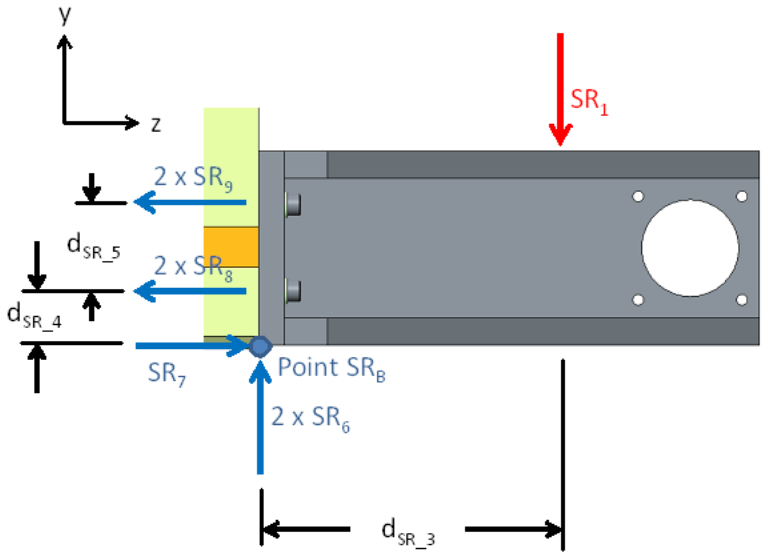

Figure D2

$d_{SR\_3} := 146.4mm = 5.764 \cdot in$

$d_{SR\_4} := 25mm = 0.984 \cdot in$

$d_{SR\_5} := 40mm = 1.575 \cdot in$

$\Sigma F_y = SR_1 - (2 \times SR_6) = 0$

$SR_6 := \frac{SR_1}{2} = 902.400 \cdot lbf$ Conservatively assume only two fasteners carry shear

$\Sigma M_{SR\_B} = -[(2 \times SR_8) \times d_{SR\_4}] - [(2 \times SR_9) \times (d_{SR\_4} + d_{SR\_5})] + (SR_1 \times d_{SR\_3}) = 0$

Assume a linear relationship between SR_8 and SR_9:

$SR_8 = SR_9 \times (d_{SR\_4})/(d_{SR\_4} + d_{SR\_5})$

Therefore,

$\Sigma M_{SR\_B} = -\{\{2 \times [SR_9 \times (d_{SR\_4})/(d_{SR\_4} + d_{SR\_5})]\} \times d_{SR\_4}\} - [(2 \times SR_9) \times (d_{SR\_4} + d_{SR\_5})] + (SR_1 \times d_{SR\_3}) = 0$

$$SR_9 := \frac{SR_1 \cdot d_{SR\_3}}{2 \cdot \left[\left(\frac{d_{SR\_4}}{d_{SR\_4} + d_{SR\_5}} \right) \left(d_{SR\_4} \right) + \left(d_{SR\_4} + d_{SR\_5} \right) \right]} = 1.771 \times 10^3 \cdot lbf$$

$$SR_8 := SR_9 \cdot \frac{d_{SR\_4}}{d_{SR\_4} + d_{SR\_5}} = 680.986 \cdot lbf$$

$$Dn_{M6} := 6mm = 0.236 in$$

$$P_{M6} := 1mm = 0.039 in$$

$$A_{M6} := 20.1mm^2 = 0.031 \cdot in^2$$

$$Dm_{M6} := Dn_{M6} - 0.9382 P_{M6} = 0.199 \cdot in$$

$$Le := 14.8mm - P_{M6} = 0.543 \cdot in$$

$$As_{M6} := \frac{\pi \cdot Dm_{M6} \cdot Le}{2} = 0.170 \cdot in^2$$

$$\tau_{thrd} := \frac{\max\left(SR_8, SR_9\right)}{As_{M6}} = 10.411 \cdot ksi$$

$$\tau_{AL6061T6\_yield} := \frac{1}{\sqrt{3}} \cdot 35ksi = 20.207 \cdot ksi$$

shear yield strength of female thread material, 6061-T6 Aluminum

$$SF_{thrd} := \frac{\tau_{AL6061T6\_yield}}{\tau_{thrd}} = 1.941$$

$Dr_{M6} := Dn_{M6} - 1.226869 \cdot P_{M6} = 0.188 \cdot in$

$Ar_{M6} := \frac{\pi \cdot Dr_{M6}^{2}}{4} - 1.94mm^{2} = 0.025 \cdot in^{2}$

$\sigma_{vm\_fast} := \sqrt{\left(\frac{\max(SR_8, SR_9)}{A_{M6}}\right)^{2} + 3 \cdot \left(\frac{SR_6}{Ar_{M6}}\right)^{2}} = 85.000 \cdot ksi$

$\sigma y_{Bumax\_109} := 130ksi$ yield strength of bracket fastener, Bumax 109

$SF_{fast} := \frac{\sigma y_{Bumax\_109}}{\sigma_{vm\_fast}} = 1.529$

Next, consider the secondary restraint posts and their mounting fasteners.

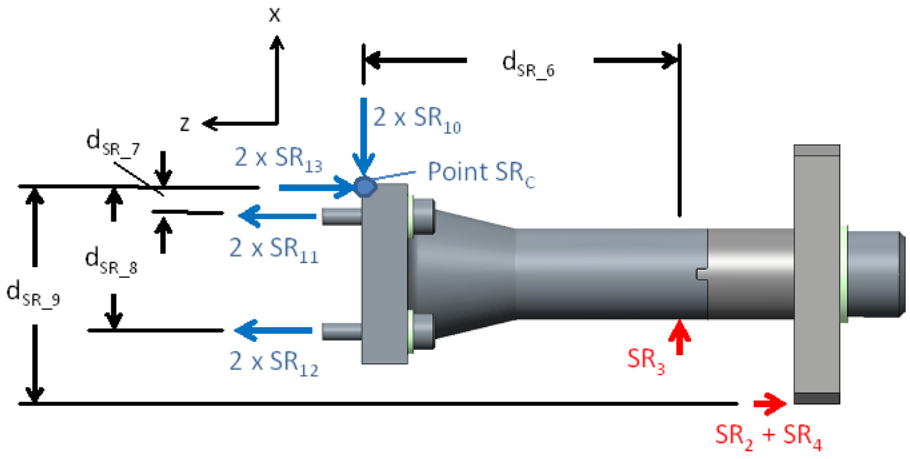

Figure D3

Note: SR_4 conservatively applied at outer edge of restraint cap

$SR_2 = 655.200 \cdot lbf$ $d_{SR\_6} := 85.7mm = 3.374 \cdot in$ distance from mount end of secondary restraint to center of Grating LRU actuator plate

$SR_3 = 777.600 \cdot lbf$ $d_{SR\_7} := 9mm = 0.354 \cdot in$

$SR_4 = 299.077 \cdot lbf$ $d_{SR\_8} := 41mm = 1.614 \cdot in$

$d_{SR\_9} := 64.1mm = 2.524 \cdot in$ includes 3mm offset for AG2/3 secondary restraints

$\Sigma M_{SR\_C} = [(SR_2 + SR_4) \times d_{SR\_9}] + (SR_3 \times d_{SR\_6}) - [(2 \times SR_{11}) \times d_{SR\_7}] - [(2 \times SR_{12}) \times d_{SR\_8}] = 0$

Assume a linear relationship between SR_{11} and SR_{12}:

$SR_{11} = SR_{12} \times (d_{SR\_7} / d_{SR\_8})$

Therefore,

$\Sigma M_{SR\_C} = [(SR_2 + SR_4) \times d_{SR\_9}] + (SR_3 \times d_{SR\_6}) - \{2 \times [SR_{12} \times (d_{SR\_7} / d_{SR\_8})] \times d_{SR\_7}\} - [(2 \times SR_{12}) \times d_{SR\_8}] = 0$

$$SR_{12} := \frac{(SR_2 + SR_4) \cdot d_{SR\_9} + SR_3 \cdot d_{SR\_6}}{2 \cdot \left(\frac{d_{SR\_7}}{d_{SR\_8}} \cdot d_{SR\_7} + d_{SR\_8} \right)} = 1.487 \times 10^3 \cdot lbf$$

$$SR_{11} := SR_{12} \cdot \frac{d_{SR\_7}}{d_{SR\_8}} = 326.415 \cdot lbf$$

$\Sigma F_x = SR_3 - (2 \times SR_{10}) = 0$

$$SR_{10} := \frac{SR_3}{2} = 388.800 \cdot lbf$$ Conservatively assume only two fasteners carry shear

$Dn_{M6} := 6mm = 0.236 in$

$P_{M6} := 1mm = 0.039 in$

$A_{M6\_vented} := 18.16mm^2 = 0.028 \cdot in^2$

$Dm_{M6} := Dn_{M6} - 0.9382 \cdot P_{M6} = 0.199 \cdot in$

$$Le := 10.7mm - P_{M6} = 0.382 \cdot in$$

$$As_{M6} := \frac{\pi \cdot Dm_{M6} \cdot Le}{2} = 0.120 \cdot in^2$$

$$\tau_{thrd} := \frac{\max\left(SR_{11}, SR_{12}\right)}{As_{M6}} = 12.439 \cdot ksi$$

$$\tau_{AL6061T6\_yield} := \frac{1}{\sqrt{3}} \cdot 35ksi = 20.207 \cdot ksi$$

shear yield strength of female thread material, 6061-T6 Aluminum

$$SF_{thrd} := \frac{\tau_{AL6061T6\_yield}}{\tau_{thrd}} = 1.625$$

$$Dr_{M6} := Dn_{M6} - 1.226869 \cdot P_{M6} = 0.188 \cdot in$$

$$Ar_{M6} := \frac{\pi \cdot Dr_{M6}^2}{4} - 1.94mm^2 = 0.025 \cdot in^2$$

accounts for vented fastener

$$\sigma_{vm\_fast} := \sqrt{\left(\frac{\max\left(SR_{11}, SR_{12}\right)}{A_{M6\_vented}}\right)^2 + 3 \cdot \left(\frac{SR_{10}}{Ar_{M6}}\right)^2} = 59.434 \cdot ksi$$

$$\sigma y_{A270} := 65ksi$$

yield strength of bracket fastener, A2-70

$$SF_{fast} := \frac{\sigma y_{A270}}{\sigma_{vm\_fast}} = 1.094$$

Next, consider stresses in the secondary restraint post. The post will be modeled as a cantilever beam. Three critical cross-sections will be analyzed.

First, consider cross-section AA:

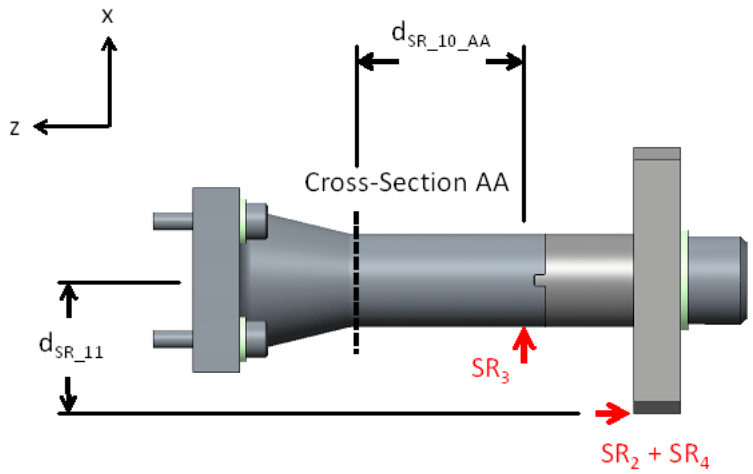

Figure D4

$d_{SR\_10\_AA} := 43.5mm = 1.713 \cdot in$

$d_{SR\_11} := 36.1mm = 1.421 \cdot in$

$d_{beam\_AA} := 25.4mm = 1.000 \cdot in$ diameter of secondary restraint post

$r_{beam\_AA} := \frac{d_{beam\_AA}}{2} = 0.500 \cdot in$ radius of secondary restraint post

$A_{beam\_AA} := \pi \cdot r_{beam\_AA}^{2} = 0.785 \cdot in^{2}$ cross-sectional area of secondary restraint post

$I_{beam\_AA} := \frac{\pi}{4} \cdot \left(r_{beam\_AA}\right)^{4} = 0.049 \cdot in^{4}$ second moment of area of secondary restraint post

$M_{beam\_AA} := SR_3 \cdot d_{SR\_10\_AA} + \left(SR_2 + SR_4\right) \cdot d_{SR\_11} = 2.688 \times 10^{3} \cdot in \cdot lbf$ bending moment applied to secondary restraint post

$F_{ten\_beam\_AA} := SR_2 + SR_4 = 954.277 \cdot lbf$ tensile load on secondary restraint post

$F_{shr\_beam\_AA} := SR_3 = 777.600 \cdot lbf$ shear load on secondary restraint post

$\sigma_{beam\_AA} := \frac{M_{beam\_AA} \cdot r_{beam\_AA}}{I_{beam\_AA}} + \frac{F_{ten\_beam\_AA}}{A_{beam\_AA}} = 28.595 \cdot ksi$ tensile stress in secondary restraint post

$\tau_{beam\_AA} := \frac{SR_3}{A_{beam\_AA}} = 0.990 \cdot ksi$ shear stress in secondary restraint post

$\sigma vm_{beam\_AA} := \sqrt{\sigma_{beam\_AA}^2 + 3 \cdot \tau_{beam\_AA}^2} = 28.646 \cdot ksi$ von Mises stress in secondary restraint post

$\sigma y_{SST304} := 30ksi$ yield strength of secondary restraint beam, 304 SST

$SF_{beam\_AA} := \frac{\sigma y_{SST304}}{\sigma vm_{beam\_AA}} = 1.047$

Next, consider cross-section BB:

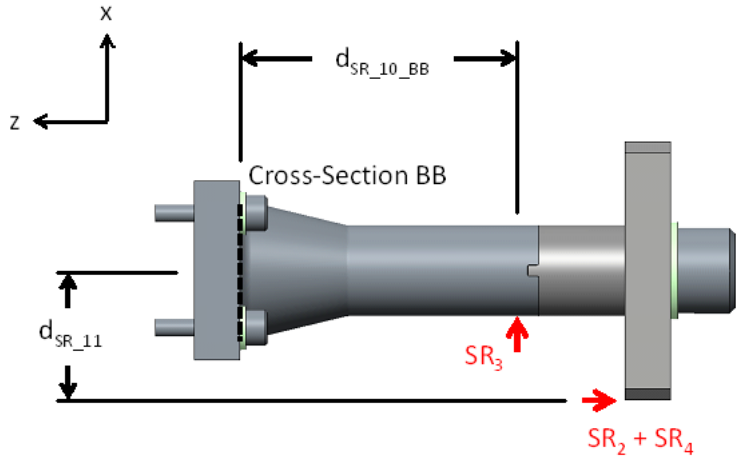

Figure D5

$d_{SR\_10\_BB} := 73mm = 2.874 \cdot in$

$d_{SR\_11} := 36.1mm = 1.421 \cdot in$

$d_{beam\_BB} := 40.0mm = 1.575 \cdot in$ diameter of secondary restraint post

$r_{beam\_BB} := \frac{d_{beam\_BB}}{2} = 0.787 \cdot in$ radius of secondary restraint post

$A_{beam\_BB} := \pi \cdot r_{beam\_BB}^{2} = 1.948 \cdot in^{2}$ cross-sectional area of secondary restraint post

$I_{beam\_BB} := \frac{\pi}{4} \cdot \left(r_{beam\_BB}\right)^{4} = 0.302 \cdot in^{4}$ second moment of area of secondary restraint post

$M_{beam\_BB} := SR_3 \cdot d_{SR\_10\_BB} + \left(SR_2 + SR_4\right) \cdot d_{SR\_11} = 3.591 \times 10^{3} \cdot in \cdot lbf$ bending moment applied to secondary restraint post

$F_{ten\_beam\_BB} := SR_2 + SR_4 = 954.277 \cdot lbf$ tensile load on secondary restraint post

$F_{shr\_beam\_BB} := SR_3 = 777.600 \cdot lbf$ shear load on secondary restraint post

$\sigma_{beam\_BB} := \frac{M_{beam\_BB} \cdot r_{beam\_BB}}{I_{beam\_BB}} + \frac{F_{ten\_beam\_BB}}{A_{beam\_BB}} = 9.856 \cdot ksi$ tensile stress in secondary restraint post

$\tau_{beam\_BB} := \frac{SR_3}{A_{beam\_BB}} = 0.399 \cdot ksi$ shear stress in secondary restraint post

$\sigma vm_{beam\_BB} := \sqrt{\sigma_{beam\_BB}^{2} + 3 \cdot \tau_{beam\_BB}^{2}} = 9.880 \cdot ksi$ von Mises stress in secondary restraint post

$\sigma y_{SST304} := 30ksi$ yield strength of secondary restraint beam, 304 SST

$SF_{beam\_BB} := \frac{\sigma y_{SST304}}{\sigma vm_{beam\_BB}} = 3.036$

Consider cross-section CC:

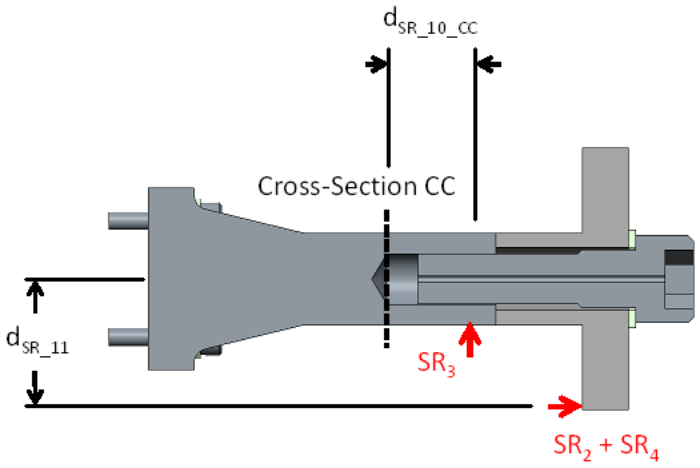

Figure D6

$d_{SR\_10\_CC} := 19.86mm = 0.782 \cdot in$ conservatively assumes full depth of tap-drilled hole

$d_{SR\_11} := 36.1mm = 1.421 \cdot in$

$d_{beam\_CC\_O} := 25.4mm = 1.000 \cdot in$ outer diameter of secondary restraint post

$d_{beam\_CC\_I} := 16.5mm = 0.650 \cdot in$ approx. inner diameter of secondary restraint post

$r_{beam\_CC\_O} := \frac{d_{beam\_CC\_O}}{2} = 0.500 \cdot in$ outer radius of secondary restraint post

$r_{beam\_CC\_I} := \frac{d_{beam\_CC\_I}}{2} = 0.325 \cdot in$ inner radius of secondary restraint post

$A_{beam\_CC} := \pi \cdot r_{beam\_CC\_O}^{2} - \pi \cdot r_{beam\_CC\_I}^{2} = 0.454 \cdot in^{2}$ cross-sectional area of secondary restraint post

$I_{beam\_CC} := \frac{\pi}{4} \cdot \left(r_{beam\_CC\_O}\right)^{4} - \frac{\pi}{4} \cdot \left(r_{beam\_CC\_I}\right)^{4} = 0.040 \cdot in^{4}$ second moment of area of secondary restraint post

$M_{beam\_CC} := SR_3 \cdot d_{SR\_10\_CC} + \left(SR_2 + SR_4\right) \cdot d_{SR\_11} = 1.964 \times 10^{3} \cdot in \cdot lbf$ bending moment applied to secondary restraint post

$F_{ten\_beam\_CC} := SR_2 + SR_4 = 954.277 \cdot lbf$ tensile load on secondary restraint post

$F_{shr\_beam\_CC} := SR_3 = 777.600 \cdot lbf$ shear load on secondary restraint post

$\sigma_{beam\_CC} := \frac{M_{beam\_CC} \cdot r_{beam\_CC\_O}}{I_{beam\_CC}} + \frac{F_{ten\_beam\_CC}}{A_{beam\_CC}} = 26.445 \cdot ksi$ tensile stress in secondary restraint post

$\tau_{beam\_CC} := \frac{SR_3}{A_{beam\_CC}} = 1.713 \cdot ksi$ shear stress in secondary restraint post

$\sigma vm_{beam\_CC} := \sqrt{\sigma_{beam\_CC}^{2} + 3 \cdot \tau_{beam\_CC}^{2}} = 26.611 \cdot ksi$ von Mises stress in secondary restraint post

$\sigma y_{SST304} := 30ksi$ yield strength of secondary restraint beam, 304 SST

$SF_{beam\_CC} := \frac{\sigma y_{SST304}}{\sigma vm_{beam\_CC}} = 1.127$

Next, consider bending in the secondary restraint end cap.

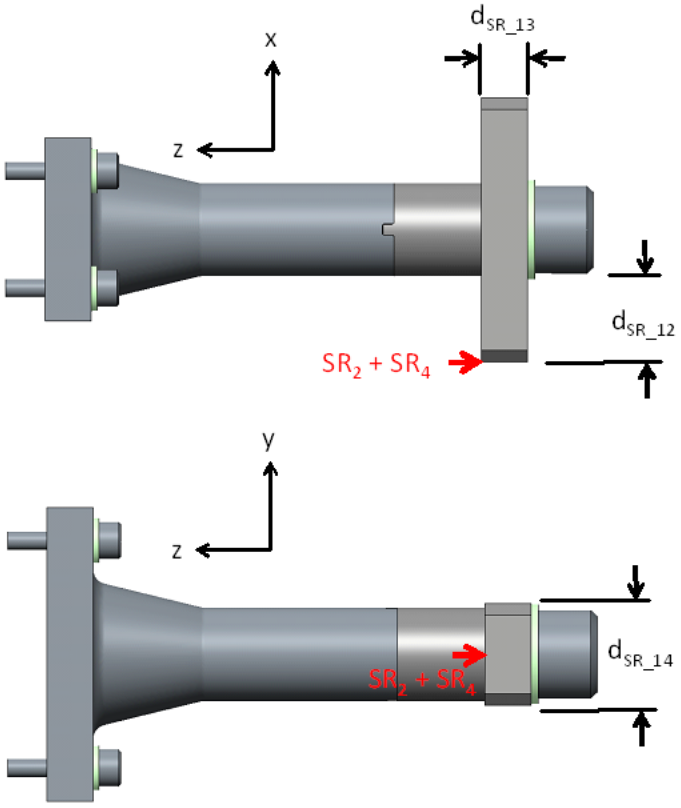

Figure D7

$SR_2 = 655.200 \cdot lbf$ $d_{SR\_12} := 22.6mm = 0.890 \cdot in$ distance from edge of restraint end cap to washer

$SR_4 = 299.077 \cdot lbf$ $d_{SR\_13} := 12.7mm = 0.500 \cdot in$

$d_{SR\_14} := 27.75mm = 1.093 \cdot in$

$c_{cap} := \frac{d_{SR\_13}}{2} = 0.250 \cdot in$ one-half of cap thickness

$A_{cap} := d_{SR\_13} \cdot d_{SR\_14} = 0.546 \cdot in^2$ cross-sectional area of secondary restraint cap

$I_{cap} := \frac{1}{12} \cdot d_{SR\_14} \cdot d_{SR\_13}^{3} = 0.011 \cdot in^{4}$ second moment of area of secondary restraint cap

$M_{cap} := (SR_2 + SR_4) \cdot d_{SR\_12} = 849.081 \cdot in \cdot lbf$ bending moment applied to secondary restraint cap

$F_{shr\_cap} := SR_2 + SR_4 = 954.277 \cdot lbf$ shear load on secondary restraint cap

$\sigma_{cap} := \frac{M_{cap} \cdot c_{cap}}{I_{cap}} = 18.652 \cdot ksi$ tensile stress in secondary restraint post

$\tau_{cap} := \frac{F_{shr\_cap}}{A_{cap}} = 1.747 \cdot ksi$ shear stress in secondary restraint post

$\sigma vm_{cap} := \sqrt{\sigma_{cap}^{2} + 3 \cdot \tau_{cap}^{2}} = 18.896 \cdot ksi$ von Mises stress in secondary restraint post

$\sigma y_{SST304} := 30ksi$ yield strength of secondary restraint beam, 304 SST

$SF_{cap} := \frac{\sigma y_{SST304}}{\sigma vm_{cap}} = 1.588$

Next, consider stresses in the M16 fastener mounting the secondary restraint cap to the post.

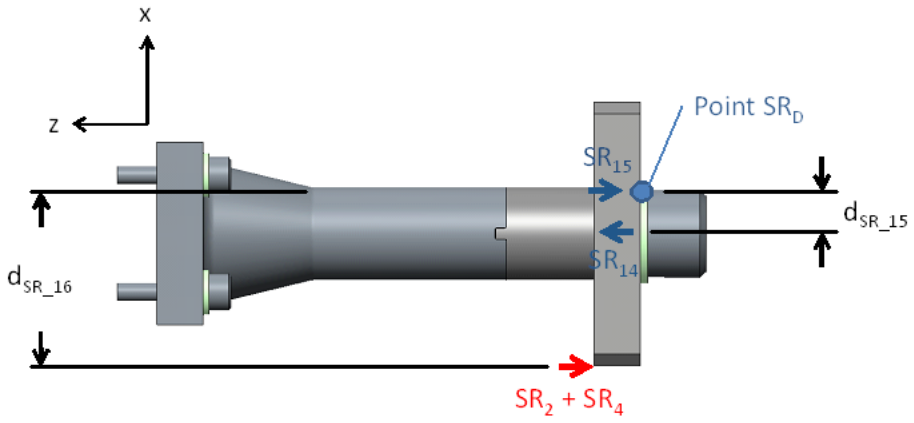

Figure D8

$SR_2 = 655.200 \cdot lbf$ $d_{SR\_15} := 12mm = 0.472in$ one half bolt head diameter

$SR_4 = 299.077 \cdot lbf$ $d_{SR\_16} := 48.8mm = 1.921in$

$\Sigma M_{SR\_D} = [(SR_2 + SR_4) \times d_{SR\_16}] - (SR_{14} \times d_{SR\_15}) = 0$

$$SR_{14} := \frac{(SR_2 + SR_4) \cdot d_{SR\_16}}{d_{SR\_15}} = 3.881 \times 10^3 \cdot lbf$$

$Dn_{M16} := 16mm = 0.630in$

$P_{M16} := 2mm = 0.079in$

$A_{M16\_vented} := 154.5mm^2 = 0.239 \cdot in^2$

$Dm_{M16} := Dn_{M16} - 0.9382 \cdot P_{M16} = 0.556 \cdot in$

$Le := 21.4mm - P_{M16} = 0.764 \cdot in$

$$As_{M16} := \frac{\pi \cdot Dm_{M16} \cdot Le}{2} = 0.667 \cdot in^2$$

$$\tau_{thrd\_2} := \frac{SR_{14}}{As_{M16}} = 5.817 \cdot ksi$$

$\tau_{304SST\_yield} := \frac{1}{\sqrt{3}} \cdot 30ksi = 17.321 \cdot ksi$ shear yield strength of female thread material, 304 SST

$$SF_{thrd\_2} := \frac{\tau_{304SST\_yield}}{\tau_{thrd\_2}} = 2.977$$

$$\sigma_{vm\_fast\_2} := \left(\frac{SR_{14}}{A_{M16\_vented}} \right) = 16.205 \cdot ksi$$

$\sigma y_{A270} := 65ksi$ yield strength of bracket fastener, A2-70

$$SF_{fast\_2} := \frac{\sigma y_{A270}}{\sigma_{vm\_fast\_2}} = 4.011$$

Appendix E – Engineering Drawings

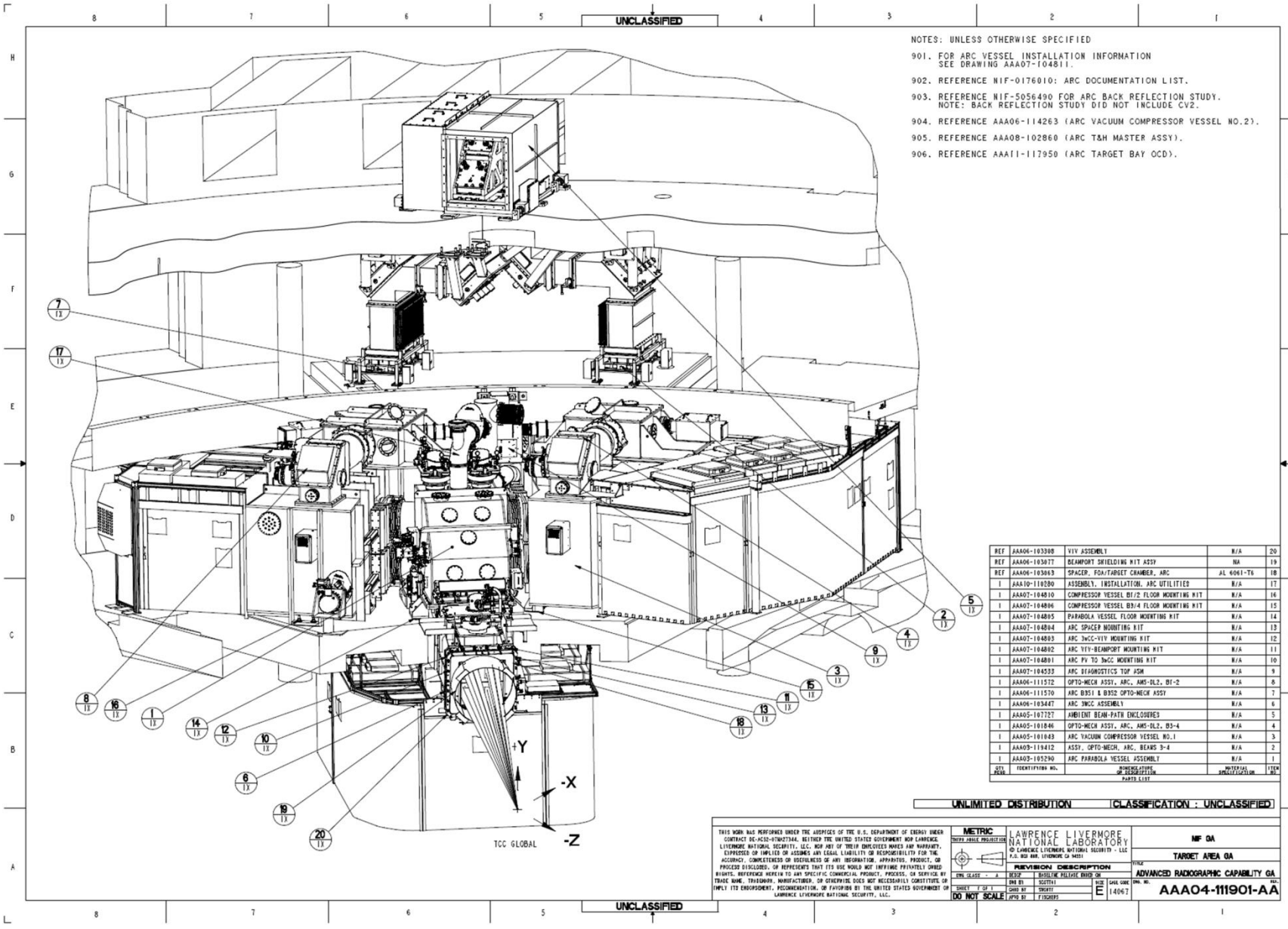

UNCLASSIFIED

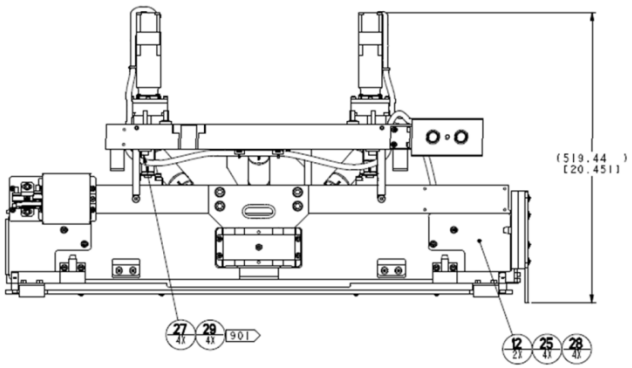

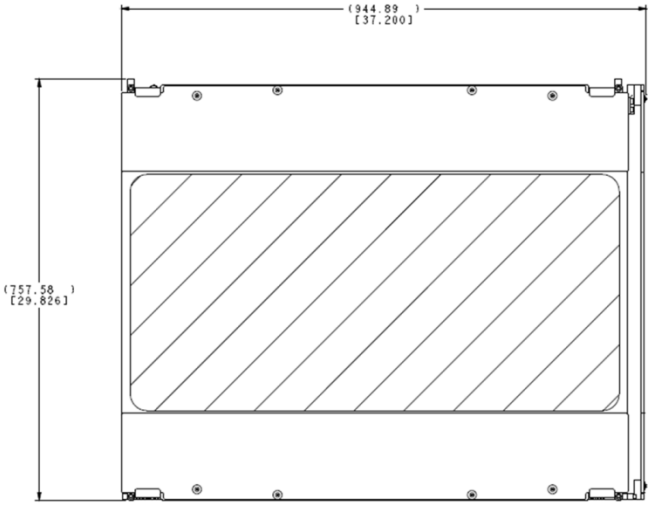

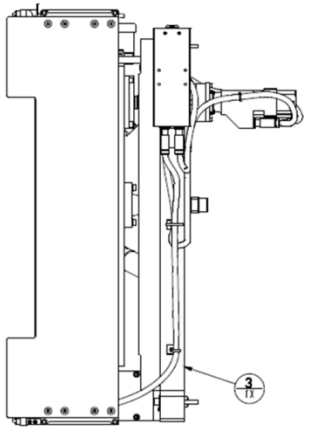

NOTES: UNLESS OTHERWISE SPECIFIED

101. ALL DIMENSIONS ARE IN MILLIMETERS (mm) AND VALUES ARE IN SI UNITS. DIMENSIONS AND VALUES IN BRACKETS ARE U.S. CUSTOMARY UNITS (inch) CONVERTED FROM MILLIMETERS / SI UNITS.

102. APPLICABLE STANDARDS AND SPECIFICATIONS:
ASME Y14.5M-1994, DIMENSIONING AND TOLERANCING
ASME Y14.38, ABBREVIATIONS AND ACRONYMS

109. ESTIMATED WEIGHT IS USING THE OPS COVER CONFIGURATION:
274.894 kg [606.038 lb] FOR TAB -01.
277.320 kg [611.386 lb] FOR TAB -02.
275.550 kg [607.488 lb] FOR TAB -03.
277.976 kg [612.832 lb] FOR TAB -04.

404 UNLESS OTHERWISE SPECIFIED BY SAFETY NOTE OR ASSEMBLY PROCEDURE, LISTED TORQUE VALUES ARE RECOMMENDED. TORQUE SST CLASS A2-70 SCREWS TO ALUM PARENT MATERIAL USING VALUE(S) INDICATED:
M5 x 0.8 4.3 N-m [38 lbf-in] (UNLUBRICATED)

901 BAG LOOSE HARDWARE FOR NEXT LEVEL ASSEMBLY.

902. ASSEMBLE HARDWARE AND APPLY PRELOAD TORQUES AS SPECIFIED IN NIF-5023177: ARC GRATING LRU ASSEMBLY PROCEDURE, NIF-5044756: ARC GRATING LRU DISASSEMBLY PROCEDURE, AND NIF-5043361: ARC COMPRESSOR VESSEL LRU T&H OPERATIONS PROCEDURE.

903 SEE SHEETS 4 AND 5 FOR ASSEMBLY OF ITEMS 18 THRU 22, AND REMOVAL OF ITEM 4. ITEM 4 IS ONLY USED DURING TRANSPORT AND HANDLING OF THE GRATING LRU.

904 ITEM 23 (GMA INSTALLATION COVER) IS ONLY USED DURING INSTALLATION AND REMOVAL OF THE GHOST MITIGATION ARMOR KITS.

905 REFERENCE: OPTIC SERIAL NUMBER MARKING IS ALWAYS LOCATED ON THE UPPER LEFT HAND SIDE OF THE GRATING ASSEMBLY.

	QTY PER TAB-04 REV.AB	QTY REQD TAB-03 REV.AD	QTY PER TAB-02 REV.AB	QTY REQD TAB-01 REV.AD	IDENTIFYING NO.	NOMENCLATURE OR DESCRIPTION	MATERIAL SPECIFICATION	ITEM NO
						TABULATED PART9 LIST		
901	4	4	4	4	N5310-10826	WSH,FLT,M8.4X25X2	SST,A2-70	29
	12	12	12	12	N5310-10750	WSH,FLT,6.4X12X1.6	SST,A2-70	28
901	4	4	4	4	N5305-45236	SCR,CAP,HXS,VNT,M8X1.25X70	SST,Ag PLD	27
	8	8	8	8	N5305-10264	SCR,CAP,HXS,VNT,M6X1X16	SST,A2-70	26
	4	4	4	4	N5305-10262	SCR,CAP,HXS,VNT,M6X1X10	SST,A2-70	25
	2	2	2	2	N5305-10243	SCR,CAP,HXS,VNTD M4 X 0.7 X 8	SST,A2-70	24
904	1	1	1	1	AAA13-113784	COVER ASSY, AG2 GMA INSTALLATION	NA	23
903	1	1	1	1	AAA13-113778	AG2 GRATING OPERATIONAL COVER ASSY	N/A	22
903	1		1		AAA13-105189	ASSY, GLASS, SIDE, AG1/AG2	N/A	21
903	2	2	2	2	AAA13-113848	ABS GLASS ASSY, AG2 FACE	N/A	20
903	1		1		AAA14-100083	GMA BRACKET KIT, AG2-B	N/A	19
903		1		1	AAA14-100082	GMA BRACKET KIT, AG2-A	N/A	18
	4	4	4	4	AAA13-110523	AG GRATING ABS, GLASS MOUNT	ALUM 6061-T6	17
	1				AAA12-110855-10	PLATE, BAR CODE, TAB-10	AL 5052-H32	16
		1			AAA12-110855-08	PLATE, BAR CODE, TAB-08	AL 5052-H32	15
			1		AAA12-110855-11	PLATE, BAR CODE, TAB-11	AL 5052-H32	14
				1	AAA12-110855-09	PLATE, BAR CODE, TAB-09	AL 5052-H32	13
	2	2	2	2	AAA11-115250	COVER	AL 6061-T6	12
404	1				AAA11-101012-02	MIRROR ASSY	N/A	11
404		1			AAA11-101012-01	MIRROR ASSY	N/A	10
404	1	1			AAA11-101011	LRU CLINOMETER ASSY W/O MIRROR	N/A	9
404			1		AAA11-101006-02	LRU CLINOMETER ASSY, W/ MIRROR	N/A	8
404				1	AAA11-101006-01	LRU CLINOMETER ASSY, W/ MIRROR	N/A	7
	1		1		LEA07-106032	RIGHT BOX KIT	N/A	6
		1		1	LEA07-106031	LEFT BOX KIT	N/A	5
903	1	1	1	1	AAA07-101911	AG2/3 GRATING COVER ASSY	N/A	4
	1	1	1	1	AAA06-103152	AG2 GRATING OPTICAL MOUNT ASSY	N/A	3
	1		1		AAA04-107724-02	GRATING, IMPRINTED - AG2, TAB-02	BRT	2
		1		1	AAA04-107724-01	GRATING, IMPRINTED - AG2, TAB-01	BRT	1

UNLIMITED DISTRIBUTION CLASSIFICATION : UNCLASSIFIED

INSTALLED TAB -02 SHOWN
SEE SUBSEQUENT PAGES FOR OTHER TABS AND CONFIGURATIONS

METRIC
THIRD ANGLE PROJECTION
DWG CLASS - A
SHEET 1 OF 6
DO NOT SCALE

LAWRENCE LIVERMORE NATIONAL LABORATORY

P.O. BOX 808, LIVERMORE CA 94551

REVISION DESCRIPTION
DESCP REVISED PER ECR 33771
DWN BY BCOTTAI
CHKD BY BHOFTI
APVD BY GALBRAITH4

SIZE E CAGE CODE 14067

ARC TARGET BAY SYSTEM ASSY
ARC OPTO-MECHANICAL ASSY
TITLE
AG2 GRATING LRU
DWG. NO. AAA07-101915-AE
REV. E

UNCLASSIFIED

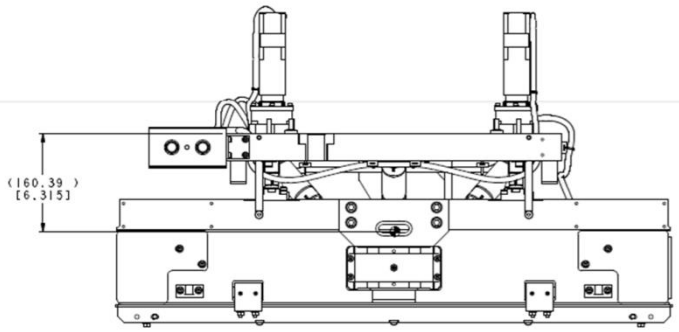

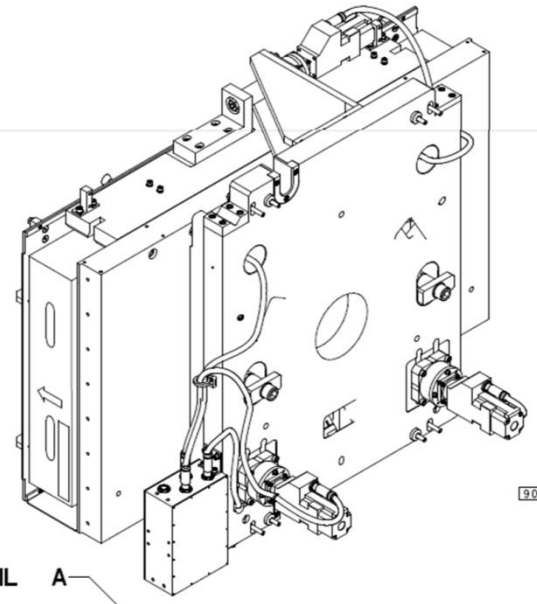

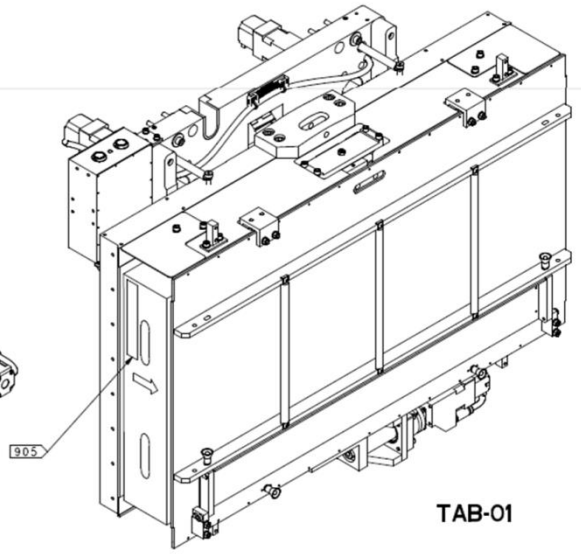

TAB-01

SEE DETAIL A

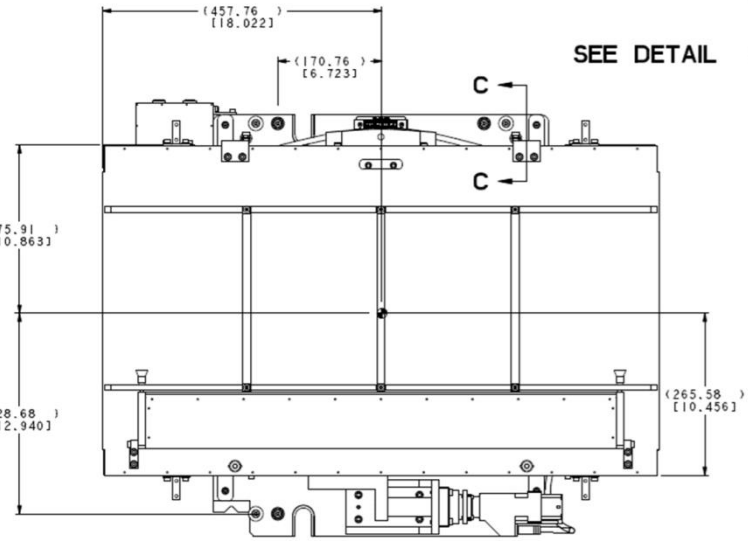

AG2 CENTER OF GRAVITY - TAB -01
TRANSPORT AND HANDLING CONFIGURATION

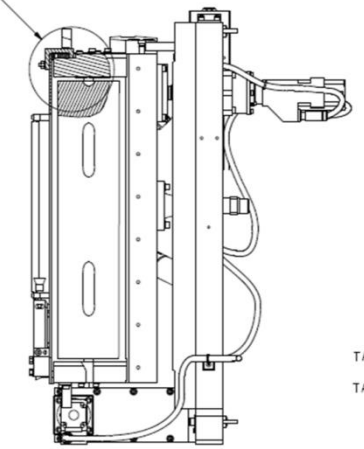

SECTION C-C

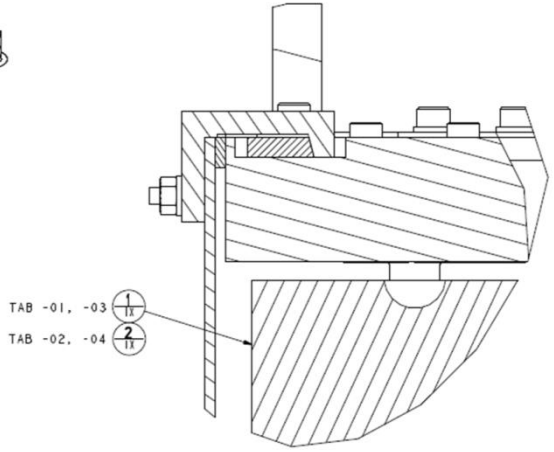

DETAIL A
SCALE 2.000

SHEET 2 OF 4	SIZE	CAGE CODE	REV. NO.
DO NOT SCALE	E	14067	AAA07-101915-AE

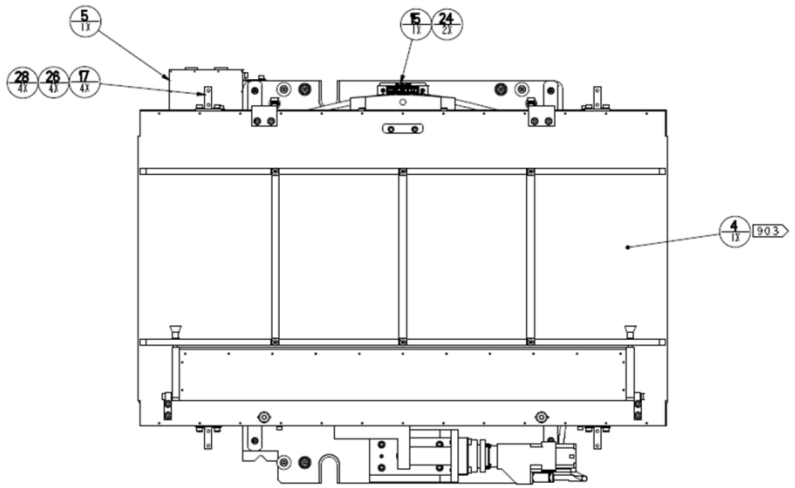

TAB-03

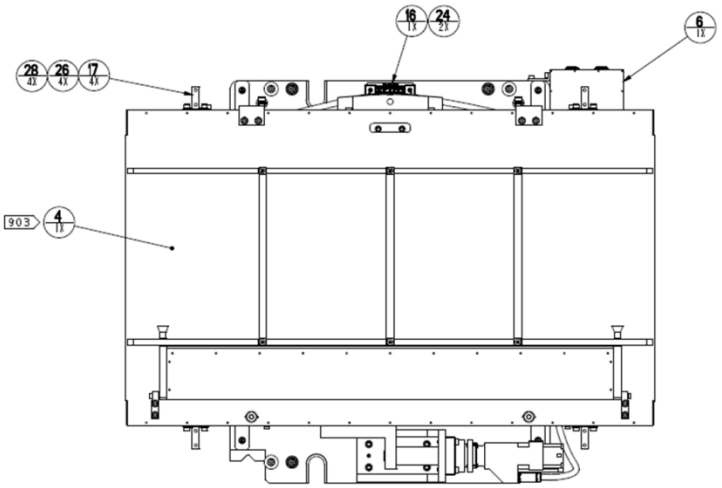

TAB-04

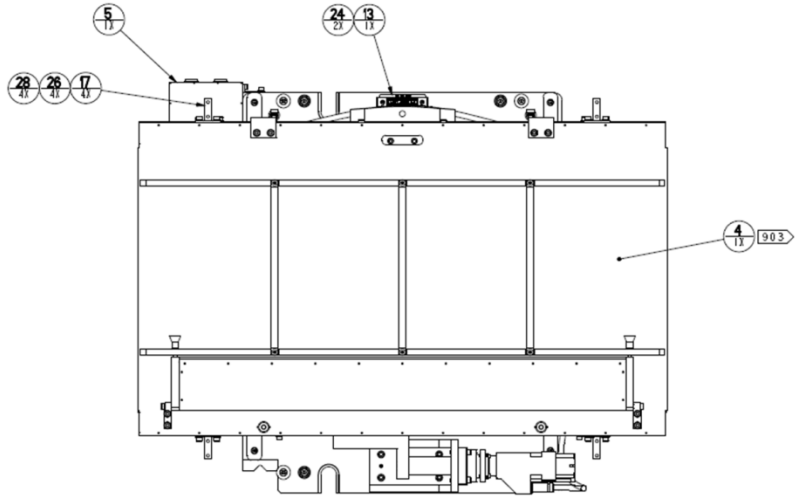

TAB-01

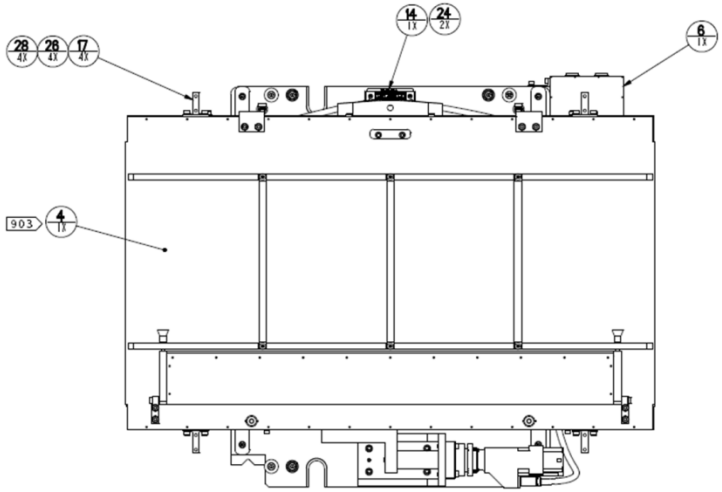

TAB-02

TRANSPORT AND HANDLING CONFIGURATION

SHEET 3 OF 3	SIZE	CAGE CODE	DWG NO.
DO NOT SCALE	E	14067	AAA07-101915-AE

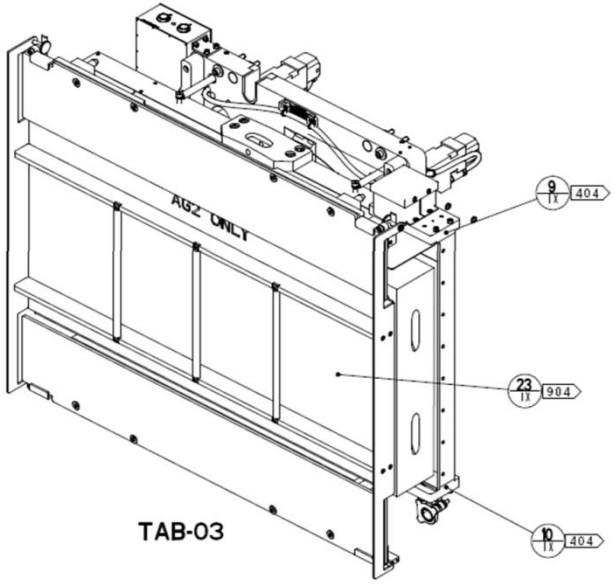

TAB-03

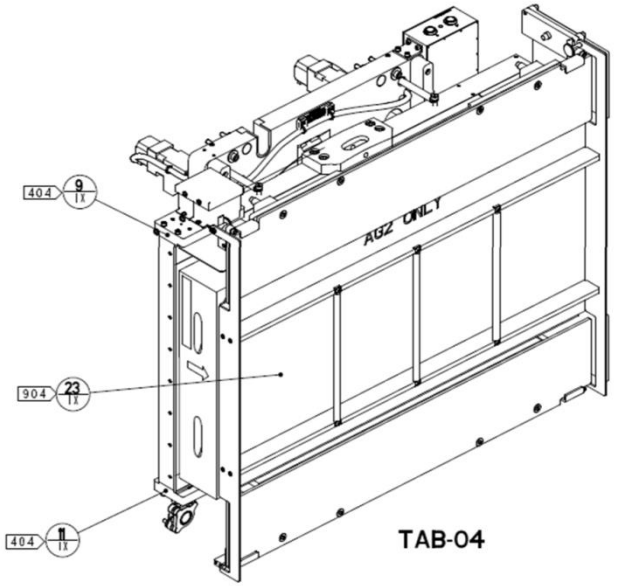

TAB-04

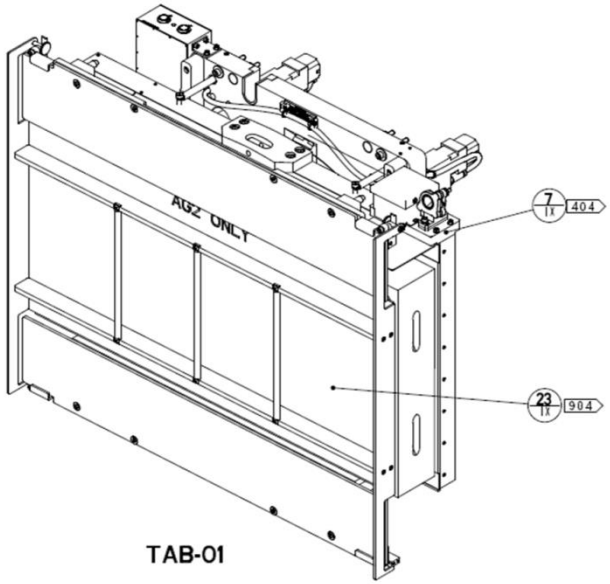

TAB-01

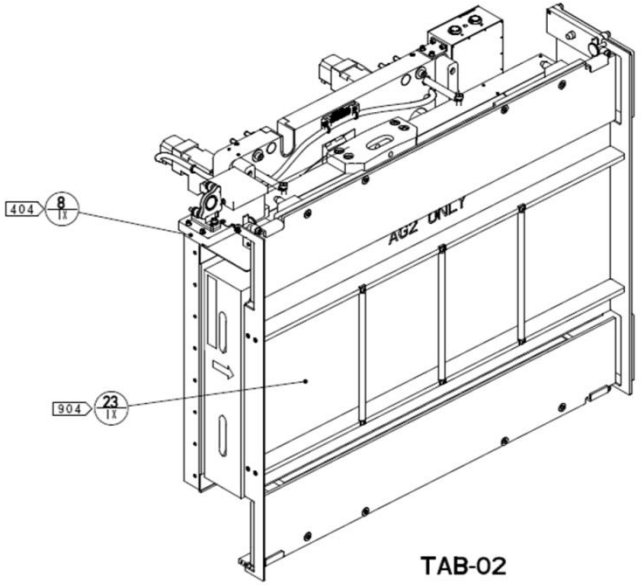

TAB-02

903

INTERMEDIATE INSTALLATION SHOWN WITH
GLASS INSTALLATION COVER (ITEM 23) INSTALLED

SHEET 4 OF 4 | DO NOT SCALE | SIZE E | CAGE CODE 14067 | DWG. NO. AAA07-101915-AE

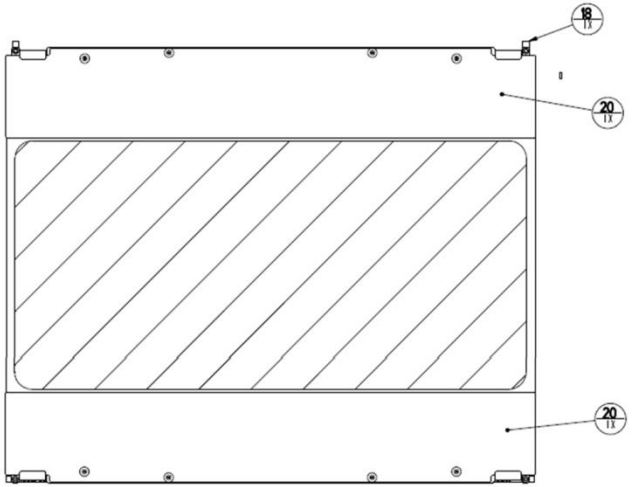

TAB-03

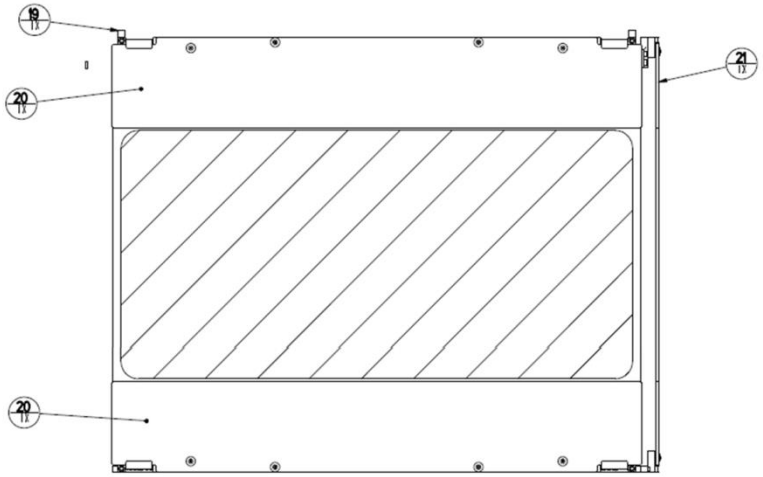

TAB-04

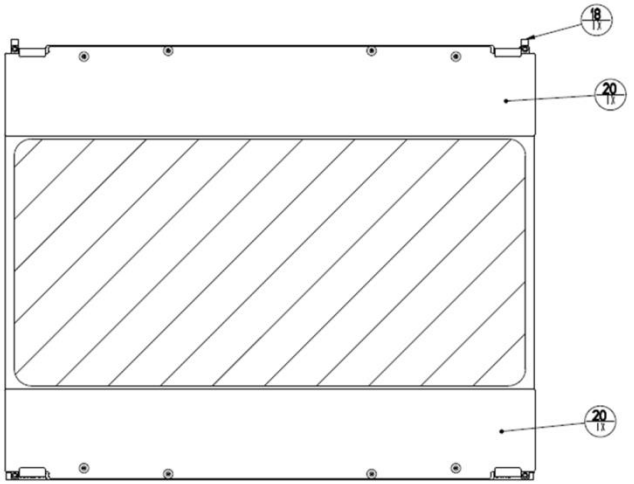

TAB-01

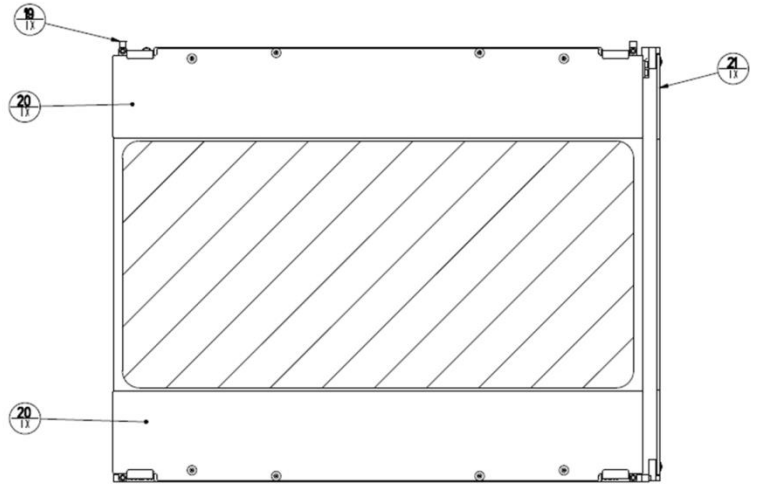

TAB-02

903

INSTALLED CONFIGURATION
(REMOVE ITEM 4 BEFORE INSTALLING THESE ITEMS)

SHEET 5 OF 6 | SIZE E | CAGE CODE 14067 | DWG NO. AAA07-101915-AE | REV

DO NOT SCALE

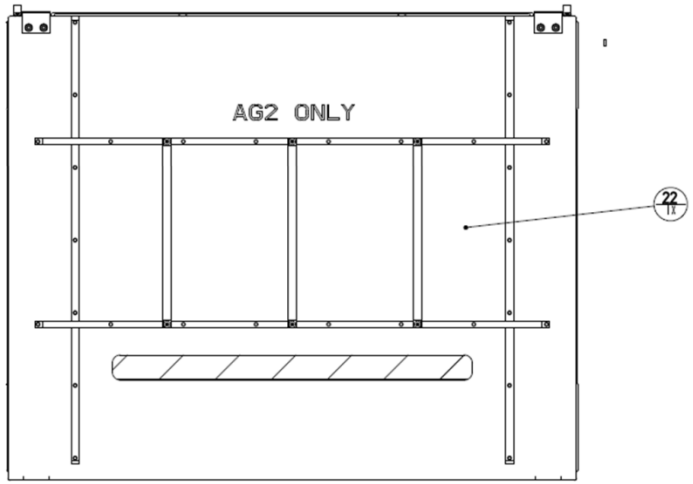

TAB-03

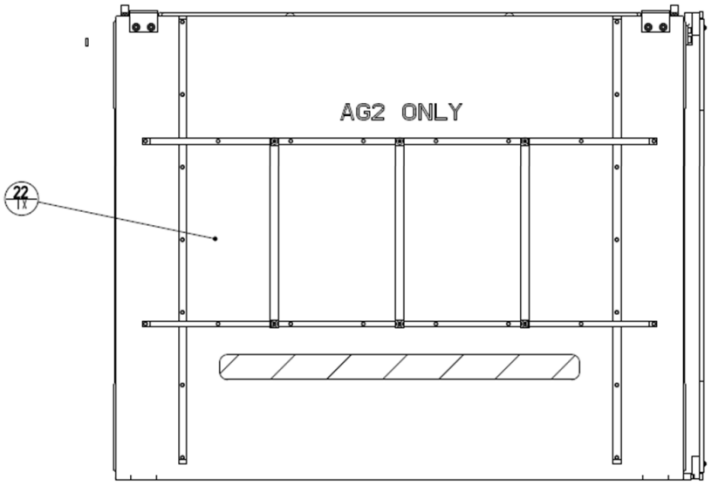

TAB-04

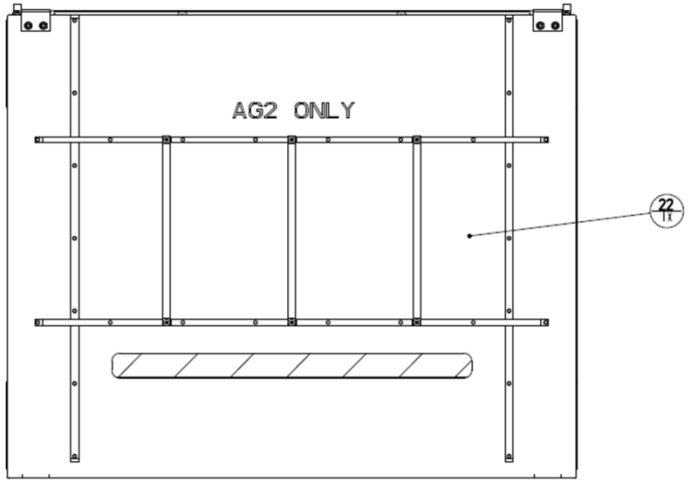

TAB-01

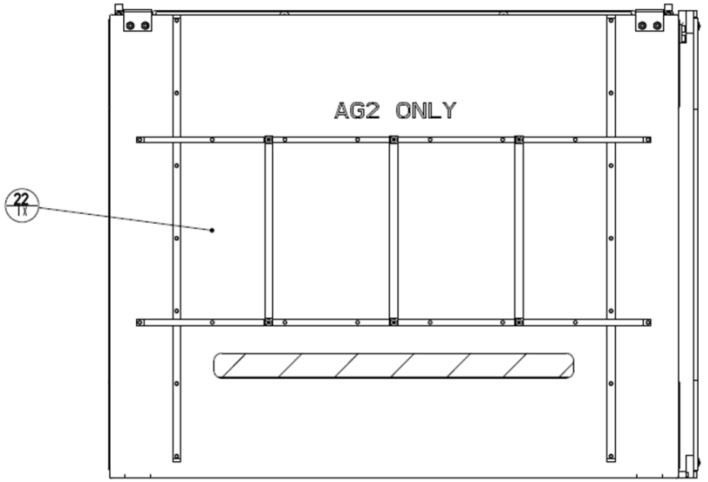

TAB-02

INSTALLED CONFIGURATION
WITH PROTECTIVE OPERATIONS COVER (ITEM 22) INSTALLED

SHEET 6 OF 6 | DO NOT SCALE | SIZE E | CAGE CODE 14067 | DWG. NO. AAA07-101915-AE | REV